Cloud droplet activity changes of soot aerosol upon smog chamber ageing

Wittbom, Cerina; Eriksson, Axel; Rissler, Jenny; Carlsson, Jonatan; Roldin, P.; Nordin, Erik; Nilsson, Patrik; Swietlicki, Erik; Pagels, Joakim; Svenningsson, Birgitta

Published in:
Atmospheric Chemistry and Physics

DOI:
10.5194/acp-14-9831-2014

2014

Atmos. Chem. Phys., 14, 9831–9854, 2014
www.atmos-chem-phys.net/14/9831/2014/
doi:10.5194/acp-14-9831-2014

Atmospheric Chemistry and Physics
Open Access

Cloud droplet activity changes of soot aerosol upon smog chamber ageing

C. Wittbom[1], A. C. Eriksson[1], J. Rissler[2], J. E. Carlsson[2], P. Roldin[1,3], E. Z. Nordin[2], P. T. Nilsson[2], E. Swietlicki[1], J. H. Pagels[2], and B. Svenningsson[1]

[1]Department of Physics, Lund University, P.O. Box 118, 221 00 Lund, Sweden
[2]Ergonomics and Aerosol Technology, Lund University, P.O. Box 118, 221 00 Lund, Sweden
[3]Department of Physics, P.O. Box 48, University of Helsinki, 00014 Helsinki, Finland

Correspondence to: C. Wittbom (cerina.wittbom@nuclear.lu.se)

Received: 14 February 2014 – Published in Atmos. Chem. Phys. Discuss.: 2 April 2014
Revised: 9 August 2014 – Accepted: 12 August 2014 – Published: 17 September 2014

Abstract. Particles containing soot, or black carbon, are generally considered to contribute to global warming. However, large uncertainties remain in the net climate forcing resulting from anthropogenic emissions of black carbon (BC), to a large extent due to the fact that BC is co-emitted with gases and primary particles, both organic and inorganic, and subject to atmospheric ageing processes. In this study, diesel exhaust particles and particles from a flame soot generator spiked with light aromatic secondary organic aerosol (SOA) precursors were processed by UV radiation in a 6 m^3 Teflon chamber in the presence of NO_x. The time-dependent changes of the soot nanoparticle properties were characterised using a Cloud Condensation Nuclei Counter, an Aerosol Particle Mass Analyzer and a Soot Particle Aerosol Mass Spectrometer. The results show that freshly emitted soot particles do not activate into cloud droplets at supersaturations ≤ 2 %, i.e. the BC core coated with primary organic aerosol (POA) from the exhaust is limited in hygroscopicity. Before the onset of UV radiation it is unlikely that any substantial SOA formation is taking place. An immediate change in cloud-activation properties occurs at the onset of UV exposure. This change in hygroscopicity is likely attributed to SOA formed from intermediate volatility organic compounds (IVOCs) in the diesel engine exhaust. The change of cloud condensation nuclei (CCN) properties at the onset of UV radiation implies that the lifetime of soot particles in the atmosphere is affected by the access to sunlight, which differs between latitudes. The ageing of soot particles progressively enhances their ability to act as cloud condensation nuclei, due to changes in: (I) organic fraction of the particle, (II) chemical properties of this fraction (e.g. primary or secondary organic aerosol), (III) particle size, and (IV) particle morphology. Applying κ-Köhler theory, using a κ_{SOA} value of 0.13 (derived from independent input parameters describing the organic material), showed good agreement with cloud droplet activation measurements for particles with a SOA mass fraction ≥ 0.12 (slightly aged particles). The activation properties are enhanced with only a slight increase in organic material coating the soot particles (SOA mass fraction < 0.12), however not as much as predicted by Köhler theory. The discrepancy between theory and experiments during the early stages of ageing might be due to solubility limitations, unevenly distributed organic material or hindering particle morphology.

The change in properties of soot nanoparticles upon photochemical processing clearly increases their hygroscopicity, which affects their behaviour both in the atmosphere and in the human respiratory system.

1 Introduction

Atmospheric aerosols are known to have a significant effect on visibility, climate and human health. Aerosol particles influence the climate and hydrological cycle of Earth by acting as cloud condensation nuclei (CCN), referred to as the indirect aerosol effect (IPCC, 2007) or the effective radiative forcing from aerosol–cloud interactions (ERFaci, IPCC, 2013). The ability of aerosol particles, to act as CCN, depends on the particle size and chemical composition as well

as the ambient water vapour supersaturation. The indirect aerosol effect includes increase in cloud albedo due to addition of cloud nuclei by pollution (Twomey, 1974), reduction of drizzle and increased cloud lifetime (Albrecht, 1989) as well as an increase in cloud thickness (Pincus and Baker, 1994). Also, soot aerosol can contribute to daytime clearing of clouds (Ackerman et al., 2000).

Soot particles make up a large fraction by number of the atmospheric aerosol, especially in urban locations in the size range < 100 nm (Rose et al., 2006, and references therein). Freshly emitted soot particles, or black carbon (BC), are known to have a predominantly warming effect on the climate due to their ability to absorb light, referred to as a direct aerosol effect (IPCC, 2007) or the radiative forcing from aerosol–radiation interactions (RFari, IPCC, 2013). Also, the absorption may increase with photochemical ageing and water uptake (Zhang et al., 2008; Cappa et al., 2012). After CO_2, BC is estimated as the strongest anthropogenic climate-forcing agent in the present-day atmosphere (Bond et al., 2013), with a total warming effect of about $+1.1\,W\,m^{-2}$ (with 90 % uncertainty bounds of $+0.17$ to $2.1\,W\,m^{-2}$). However, BC also has an effect on the Earth's hydrological cycle. According to Bond et al. (2013) the largest uncertainties in net climate forcing are related to the lack of knowledge about cloud interactions with BC when co-emitted with organic carbon (OC).

Soot is not only present close to sources, but can be transported long distances. The warming effect of soot in the Arctic has recently gained increased interest, both due to transport of soot from urban areas and also due to possible future soot emissions in the Arctic area from ship traffic which is made possible due to the reduction in ice coverage. The enhanced light absorption by soot, due to condensing material during photochemical ageing, may influence and boost the warming of the surroundings even further. Also, soot deposited on snow and ice may enhance surface heating and ice melting by decreasing the surface albedo (e.g. Bond et al., 2013; Tunved et al., 2013, and references therein). The particle number concentration is in general low (about a couple of hundred cm^{-3}) in the Arctic (Tunved et al., 2013). Wet removal and photochemical ageing play central roles in controlling the aerosol size distribution properties during the Arctic summer. As pointed out by Tunved et al. (2013), it is highly relevant to obtain a better understanding of the microphysical properties of the different aerosol populations abundant in the Arctic environment, in order to improve the understanding of the direction and magnitude of a future climate change in the region.

According to the World Health Organization (WHO, 2012), emissions of diesel engine exhaust are classified as carcinogenic in humans in addition to being linked with climate change. The unfavourable health effects caused by exposure to diesel exhaust are described in several studies (e.g. Sydbom et al., 2001; Mills et al., 2007; Hart et al., 2009). The deposited fraction in the human respiratory system is well described by the mobility diameter (for particles < 400 nm), whilst deposited dose by surface area and mass require knowledge of the characteristics of the particles due to their agglomerated structure (Rissler et al., 2012). The particle lung deposition is substantially altered by hygroscopicity (Löndahl et al., 2009). A change towards more hygroscopic properties will shift the deposited fraction in the respiratory tract towards larger sizes. Photochemical processing of diesel exhaust particles thereby alters the uptake in the human respiratory system due to enhanced hygroscopicity.

Diesel exhaust aerosol is formed during combustion processes mainly of refractory carbonaceous material (BC) that is highly agglomerated, primary organic compounds in the particle phase and volatile organic compounds (VOCs) in the gas phase. There is no clear definition for soot formed from incomplete combustion, however in general soot consists of roughly eight parts of carbon and one part of hydrogen by atoms (Tree and Svensson, 2007). In this study the term soot particles refers to the agglomerated particles emitted from diesel vehicles or by a soot generator, including both BC and organic carbon (Petzold et al., 2013). Diesel exhaust particles (DEPs) and soot generator particles (FSPs) refer to particles from the diesel vehicle and the flame soot generator respectively.

Freshly emitted soot particles are hydrophobic or limited in hygroscopicity and unlikely to contribute to the CCN population in the atmosphere (Weingartner et al., 1997; Meyer and Ristovski, 2007; Zhang et al., 2008; Tritscher et al., 2011). The size of these non-spherical particles will normally differ between measurement techniques (DeCarlo et al., 2004), for example, showing a larger mobility than volume-equivalent diameter. However, as the soot particles reside in the atmosphere, they undergo physical and chemical changes during UV exposure – they age. The agglomerated soot particles are exposed to chemical gas-to-particle processes in the atmosphere, resulting in condensation of organic and inorganic (Rose et al., 2006) vapours and coagulation of particles onto the agglomerates. Due to this ageing process the soot particles collapse into a more compact structure (Weingartner et al., 1997; Pagels et al., 2009; Tritscher et al., 2011). Hygroscopicity is enhanced with increasing ageing time, affected by high sulfur content in the fuel, high VOC levels in the emissions, pre-treatment of the exhaust gas with ozone, and UV radiation (e.g. Weingartner et al., 1997; Tritscher et al., 2011). Weingartner et al. (1997) proposed that diesel exhaust aerosol, which was pre-treated with O_3 and then subjected to UV radiation, would show an enhancement in hygroscopicity. However, the large scatter in data made it impossible to draw conclusions. Soot agglomerates become more hygroscopic when coated, partly or fully, by organic or inorganic material. The coating material transforms the agglomerates to enable them to act as CCN.

In the atmosphere in general, aerosol particles are composed of both organic and inorganic compounds. Organic material makes up a significant fraction (20 to 90 %) of the

submicrometre aerosol mass in many locations (Kanakidou et al., 2005; Jimenez et al., 2009). Organic aerosol is either introduced into the atmosphere from primary sources (i.e. primary organic aerosol, POA) or formed in the atmosphere via complex gas–particle conversion processes forming secondary organic aerosol (SOA). SOA can be formed when VOCs, either from biogenic or anthropogenic sources, are present. Oxidation products from the VOCs condense and produce SOA. The condensation of oxidised VOCs alters the particle properties, which may lead to an increased ability of the particle to act as CCN – though organic compounds will typically not improve the water activity as much as inorganic salts. Previous studies of biogenic SOA have shown that aerosol yield and hygroscopicity of SOA are dependent on experimental conditions (e.g. Asa-Awuku et al., 2009; Frosch et al., 2013). For example, hygroscopicity strongly depended on exposure to OH, with less hygroscopic particles in the presence of an OH scavenger than in experiments with OH present.

Köhler theory (Köhler, 1936) is commonly used to predict and describe the ability of the particles to activate into cloud droplets (further described in Sect. 3). However, the activation of particles in complex mixtures, in ambient air, is problematic to explain in theory (e.g. Laaksonen et al., 1998; Svenningsson et al., 2006). Previous work regarding the activation properties and processes of organic aerosols in reaction chambers, often studied SOA from biogenic precursors such as limonene, α-pinene and β-caryophyllene – Prenni et al., 2007 (α-pinene, β-pinene, $\Delta 3$-carene, and toluene); Duplissy et al., 2008 (α-pinene); Kundu et al., 2012 (limonene); Frosch et al., 2013 (β-caryophyllene).

Rissler et al. (2006) first introduced the hygroscopicity parameter κ (H-TDMA-derived), describing the number of ions or non-dissociating molecules per unit volume of the dry particle. A very similar parameter, also denoted κ, was later introduced by Petters and Kreidenweis (2007). This κ parameter is in principle the same as the κ introduced by Rissler et al. (2006), differing only due to different choice of units (Rissler et al., 2010). Since the one introduced by Petters and Kreidenweis (2007) is more broadly used and reported in the literature this one will be reported here and is the one referred to from now on. This hygroscopicity parameter ranges from 0.5 to 1.4 for salts such as NaCl that are highly CCN-active. Slightly to very hygroscopic organic species have κ values between 0.01 and 0.5, and non-hygroscopic components have a $\kappa = 0$ (such as untreated soot particles; e.g. Henning et al., 2012). κ has previously been reported to be in the range 0–0.13 (apparent κ) for photochemically aged diesel soot, and for SOA from pure gas phase of the diesel vehicle in the range 0.09–0.14 (Tritscher et al., 2011). These values could be compared to κ values for aged biogenic SOA; for β-caryophyllene SOA κ is 0.002–0.16 (e.g. Huff Hartz et al., 2005; Asa-Awuku et al., 2009; Frosch et al., 2013), and for α-pinene $\kappa = 0.1$ (e.g. Prenni et al., 2007; Duplissy et al., 2008). Dusek et al. (2006) calculated κ values for air masses in the range 0.15–0.30, originating from four different places but arriving in the same area. Not many studies have been performed concerning how the ageing process affects the activation properties of soot particles into cloud droplets and the few previous studies performed have not been able to capture the rapid change of the particle properties and improved activation (e.g. Tritscher et al., 2011).

The aim of this study is to experimentally examine the change in cloud activation properties of photochemically processed soot and evaluate the results using κ-Köhler modelling. We present results from scanning flow CCN analysis (SFCA), enabling high temporal and supersaturation resolution. Linked to the activation properties are results from online measurements of the chemical composition of the particles (soot core and organic coating), evaluated through online mass spectrometry. Also used in the evaluation is the knowledge about the change in shape and morphology of the particles, determined from the particle mass–mobility relationship. The change in particle properties (chemical composition, shape and morphology) during ageing has also been used for modelling the critical supersaturation (s_c) of the coated soot particles.

2 Experimental

Ageing experiments of soot aerosols and precursors were carried out in the smog chamber in the aerosol laboratory at Lund University (LU). In total six experiments were evaluated and presented in this study, chosen by coverage in data. The photochemical ageing was induced using black lights (peak at 354 nm) in a 6 m^3 Teflon/FEP bag. The experimental set-up is described elsewhere (Nordin et al., 2013). An overview of the experiments performed is given in Table 1.

Here we present the results from experiments where two sources of primary aerosol were used, soot agglomerates from (1) a Euro II Diesel Passenger Vehicle (VW Passat 1998) and (2) a diffusion flame soot generator described in detail elsewhere (Malik et al., 2011). The soot nanoparticles and gases from the vehicle were transferred from the tailpipe via a heated inlet system using an ejector diluter (DI-1000, Dekati Ltd Finland), with a modified inlet nozzle to achieve a primary dilution ratio of 4.5, into the initially clean smog chamber (particle number and volume concentrations $< 100\,cm^{-3}$ and $< 0.01\,\mu g\,m^{-3}$, respectively). For the pressurised air, supplying the ejector and all other pressurised air applications in the chamber, a special filter configuration was used. In short, the pressurised air was preheated to 140 °C and passed through multiple filter sets to remove particles, organic acids, NO_x, SO_x and O_3. Total dilution ratios of ~ 350 for the diesel vehicle and 50–100 for the flame soot generator were finally achieved in the Teflon chamber, depending on the injection time of the exhausts. This corresponds to number concentrations of 6000–12 000 cm^{-3} and mass concentrations of 3–14 $\mu g\,m^{-3}$.

Table 1. Experimental details of the dry particle mobility diameter ($d_{m,dry}$), the primary particle diameter (d_{pp}), the critical supersaturation measured by the two different CCNC instruments (s_c, #52 and s_c, #53), and CCNC operational mode: conventional (ΔT-stepwise) or scanning flow (SFCA).

Exp.	Source	$d_{m,dry}$ [nm]	d_{pp}^{a} by number (by mass) [nm]	d_{pp}^{b} by number (by mass) [nm]	s_c (#52) [%]	s_c (#53) [%]	CCNC operation mode
DEP1	Diesel exhaust, BTX	150	28 ± 8 (35)	30 (37)	0.18–1.8	–	ΔT-stepwise
DEP2	Diesel exhaust, TX	150	28 ± 8 (35)	28 (35)	0.18–2.05	–	SFCA
DEP3	Diesel exhaust, TX	Whole aerosol	28 ± 8 (35)	29 (36)	0.54–1.79	0.50–0.69	SFCA
DEP4	Diesel exhaust, TX	90	28 ± 8 (35)	28 (35)	0.25–0.88	0.39-0.81	SFCA
		150	28 ± 8 (35)	28 (35)	0.19–1.50	0.19–0.41	
		300	28 ± 8 (35)	28 (35)	0.07–0.65	–	
		400	28 ± 8 (35)	28 (35)	0.07	–	
FSP1	Soot generator, TX	90	–[c]	27 (34)	1.40–1.79	0.39–0.69	SFCA
		150	–[c]	27 (34)	0.18–0.82	0.19–0.95	
		300	–[c]	27 (34)	0.08–0.09	0.08	
FSP2	Soot generator, TX	60	–[c]	18 (22)	0.78–1.56	0.76-0.96	SFCA
		90	–[c]	18 (22)	0.61–2.03	0.53–0.63	
		150	–[c]	18 (22)	0.28–1.16	0.36–1.21	

[a] TEM image analysis (Rissler et al., 2013).
[b] Calculated according to Rissler et al. (2013).
[c] TEM samples missing.

By changing the air-to-fuel ratio in the flame soot generator, particles with primary particle sizes of ~ 18 and ~ 27 nm were generated (calculated according to Rissler et al. (2013), see Sect. 5.1 for more details). In all experiments, selected amounts of toluene and *m*-xylene (at a ratio of 2 : 1) were added to allow investigations of the early ageing as well as the full transformation of BC from agglomerates to spheres. Toluene and *m*-xylene are anthropogenic SOA precursors commonly found in diesel and gasoline exhaust. The initial amount of VOCs was 300–900 ppb. The NO level after exhaust injection was $\sim$ 500–600 ppb. Ozone was used to titrate NO down to a concentration of about 50 ppb before the onset of UV radiation. This also allowed us to investigate the effects of addition of ozone on CCN properties of soot.

2.1 Instrumentation

For monitoring the soot transformation during ageing a comprehensive instrumental set-up was used, shown schematically in Fig. 1.

The cloud-activation properties were measured using continuous-flow streamwise thermal-gradient CCN counters (CFSTGC from DMT, CCNC-100, DMT, described by Roberts and Nenes, 2005; and Lance et al., 2006). In the CCNC a single supersaturated column and an optical particle counter (OPC) are used for measurements of CCN. Supersaturation is achieved via a vertical thermal gradient through the column (change of temperature) and can be set to a range of 0.07–2 %, according to the manufacturer. The column is continually wetted and the instrument keeps a continuous flow. A differential mobility analyser (DMA) was placed prior to the CCNC, enabling a size selection of the dry, quasi-monodisperse aerosol particles according to their mobility diameter (d_m).

In short, the operation principle in the CCNC is that diffusion of water vapour is faster than diffusion of heat in air. The temperature and water vapour concentration will travel from different distances upwind from the walls to points along the symmetry axis in the centre of the column. Water diffuses more quickly than heat. Hence, there is more water vapour available than thermodynamically allowed at the points along the symmetry axis. Sample air passes along this axis surrounded by sheath air.

Experiments were performed during two separate campaigns. During the first campaign (experiment DEP1, Table 1), the supersaturation change was induced in a "conventional" manner (for $s_c < 1$ %): the flow is kept constant, while the temperature gradient is varied in a stepwise way. Also, the mobility diameter (d_m) was kept constant. Due to the slow temperature stabilisation, measurement of complete supersaturation spectra is time consuming. To capture the $s_c > 1$ % in the experiment DEP1, both the supersaturation (1.8 %) in the CCNC as well as d_m (150 nm) was kept constant, allowing the ageing of the aerosol scan past the supersaturation to capture the point of activation. The residence time in the CCNC is $\sim$ 6–12 s.

However, during the second campaign the Scanning Flow CCN Analysis (SFCA, introduced and described in detail by Moore and Nenes, 2009) was introduced (DEP2–4 and FSP1–2, Table 1). This altered way of operation enables rapid and continuous measurements of the supersaturation spectra. By adding a small software change to the robust and

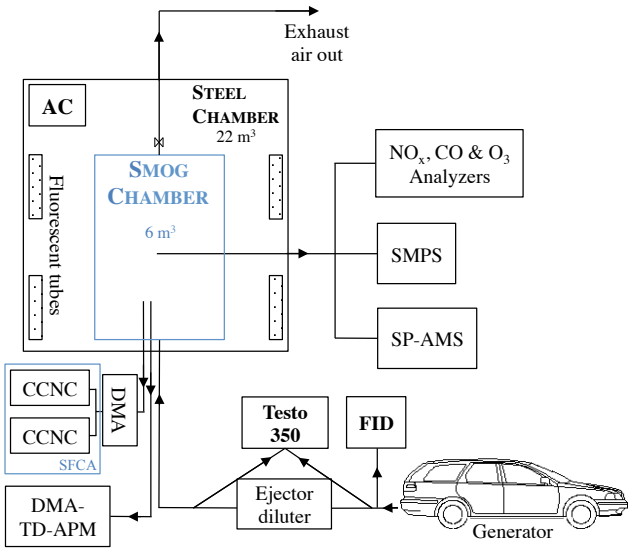

Figure 1. Schematic illustration of the instrumental set-up. Two sources of particles were examined: soot from (1) a Euro II Diesel Passenger Vehicle and (2) a Flame Soot Generator. The photochemical ageing was induced using black lights (peak at 354 nm) in a 6 m^3 Teflon/FEP bag inside the steel chamber. Two cloud condensation nucleus counters (CCNCs, DMT 100), running in parallel in SFCA operational mode, measured the cloud-activation properties (for all experiments except DEP1). The Aerosol Particle Mass Analyzer (APM, Kanomax Japan 3600) characterised the particle mass–mobility relationship. Both instruments measured the exhaust aerosol after mobility size selection by a differential mobility analyser (DMA). A scanning mobility particle sizer (SMPS) system monitored the particle number size distribution. The chemical composition of the particles was determined using a Soot Particle Aerosol Mass Spectrometer (SP-AMS, Aerodyne Research).

well-established hardware of the CCNC, the flow is instead varied through the column in a controlled manner, while the streamwise temperature gradient (ΔT) and pressure (P) is maintained constant. A higher flow increases the difference in travel distances between water and heat, and thereby increases the supersaturation. The flow rate in the chamber is varying in a scan cycle, where the flow increases/decreases linearly (for 120 s), as well as being briefly kept constant at maximum/minimum flow rates (for 20 s).

When calibrating the instrument a size-selected aerosol of well-known chemistry is used, here ammonium sulfate and sucrose. The flow and the corresponding activated fraction of the particles generate a supersaturation curve with a "critical flow rate", Q_{50}. From knowledge of the particle dry diameter and chemical composition Q_{50} is translated to a critical supersaturation (s_c) using Köhler theory. Hence, every instantaneous flow rate corresponds to a critical supersaturation (see calibration curves for one of the CCNCs, Supplement, Fig. S1). However, the calibration curves are specific for the chosen ΔT, scan time and pressure. The calibration curves are presented with error bars representing 95 % confidence intervals. SFCA enables measurements of many supersaturation spectra during a short time period, allowing a better temporal resolution. The inlet temperature can be kept closer to ambient conditions, therefore minimising biases from volatilisation of semi-volatile compounds in the instrument (Moore and Nenes, 2009).

To capture the whole supersaturation spectra of the ageing soot agglomerates, three values of ΔT were used ($\Delta T = 18$, 10, and 4 K). Two CCNC instruments were running in SFCA mode in parallel after a DMA. Hence, the two instruments were measuring the same d_m, but with overlapping ΔT. The size selection in the DMA is given in Table 1. The rapid and continuous measurements of the supersaturation spectra made it possible to capture the change in activation due to the fast ageing of the soot agglomerates. By running the CCNC instruments in parallel with inverse scan cycles, i.e. with one instrument at maximum flow rate and the other at minimum, the aerosol flow was kept constant (1 L min^{-1}).

The particle mass–mobility relationship of individual particles was measured using an Aerosol Particle Mass Analyzer after size selection with a Differential Mobility Analyser (DMA-APM; McMurry et al., 2002; Kanomax Japan 3600). The increasing mass fraction of condensed material on soot particles undergoing changes in morphology was quantified using the approach introduced by Pagels et al. (2009). A thermodenuder was introduced between the DMA and APM (Malik et al., 2011), hence a DMA-TD-APM. The thermodenuder operated at 300 °C. By comparing measurements with and without thermodenuder it was possible to quantify the size-dependent mass fraction condensed onto the non-volatile soot cores. For calculations of the volume-equivalent diameter (d_{ve}), the peak of the mass distribution was used. An example of operational details is found in the Supplement (Table S1) and a more detailed description of the operational procedure and calculations are found elsewhere (Rissler et al., 2013, 2014).

A custom-built scanning mobility particle sizer (SMPS) system (Löndahl et al., 2008) was used for measuring the particle number size distribution from about 10 to 600 nm. The SMPS system consists of a DMA (Vienna, 0.28 cm long), a ^{63}Ni bipolar charger and a condensation particle counter (CPC, model 3010, TSI Inc., USA) with a sheath/aerosol flow relationship of 4.9/0.7 dm^3 min^{-1}.

The chemical composition of the particles (soot core and organic coating) was determined using an online Aerodyne high-resolution time-of-flight mass spectrometer (HR-ToF-AMS, Aerodyne Research). For detection of refractory black carbon (rBC) the instrument was equipped with a laser vaporiser, which is referred to as a Soot Particle Aerosol Mass Spectrometer (SP-AMS, Aerodyne Research). The laser was operated in 5 min periods every hour, while the tungsten vaporiser (used in an (non-SP) AMS) was engaged continuously. The 5 min intervals were used to estimate the organic aerosol (OA) mass fraction (mf_{OA}), further described in the Supplement. The tungsten vaporiser data were only used to

Table 2. Input values for CCN modelling. The values for SOA and POA are independently retrieved from measurements, modelling and previous studies (see references in Sect. 4).

	Water	SOA	POA	BC
M(kg mol^{-1})	0.018153	0.2	0.4	
ρ (kg m^{-3})	997.1	1400	800	1850
i	–	1	0	0
σ (N m^{-1})	0.072	0.072*	0.072*	
κ	–	0.1265	0	0
T (K)	298.15			

* In solution with water.

study the chemical composition of the OA. Both instrument configurations are described elsewhere (DeCarlo et al., 2006; Onasch et al., 2012).

High-resolution transmission electron microscopy (HR-TEM) image analysis of the soot agglomerates to determine primary particle size and soot microstructure has been performed and is described elsewhere (Rissler et al., 2013). In short, soot was deposited onto lacey carbon coated copper TEM grids, using an electrostatic precipitator (NAS model 3089, TSI Inc., operated at 9.6 kV, 1 lpm), and then analysed using an HR-TEM (JEOL 3000 F, 300 kV) equipped with a field emission gun.

For general monitoring as well as for detailed chemistry modelling (not included in this study) NO_x, O_3, CO, RH, temperature, differential pressure, and UV intensity were continuously monitored throughout the experiment. Furthermore, in selected experiments a Proton Transfer Reaction Mass Spectrometer (PTR-MS, Ionicon Analytik GmbH, Austria) was used for monitoring of time-resolved VOC concentration (light aromatic compounds and other selected VOCs). The monitoring instruments as well as the SMPS and AMS are further described by Nordin et al. (2013).

3 Theory

Theoretical calculations of the critical supersaturations for the CCN activation of the soot particles coated with different organics have been performed using Köhler and κ-Köhler theory. The Köhler theory describes the saturation ratio, s, over an aqueous solution droplet as (Pruppacher and Klett, 1997; Seinfeld and Pandis, 2006)

$$s = \frac{p}{p_0} = a_w \times \mathrm{Ke}. \quad (1)$$

The saturation ratio is defined as the ratio of the actual partial pressure of water (p) to the equilibrium pressure over a flat surface of pure water (p_0), at the same temperature. The activity of water in solution is described by the term a_w, and Ke (the so-called Kelvin effect) determines the effect the surface curvature has on the equilibrium water vapour pressure. The Kelvin term is given by

$$\mathrm{Ke} = \exp\left(\frac{4\sigma_{sol}M_w}{RT\rho_w D_{wet}}\right), \quad (2)$$

where σ_{sol} is the surface tension of the droplet solution, M_w and ρ_w is the molar weight and density of water, R is the universal gas constant, T is the absolute temperature and D_{wet} is the diameter of the spherical aqueous solution droplet (input values are listed in Table 2). In the basic equation, an approximation is made of the partial molar volume of water by the molar volume of pure water (Kreidenweis et al., 2005). In this study σ_{sol} is parameterised by the surface tension of water (σ_w), with a constant value of 0.072 N m^{-1}. The activity of water (a_w) can be described by the following form of Raoult's law, where the van't Hoff factor (i_s) represents the effects of ion interactions and dissociation (Kreidenweis et al., 2005; Rose et al., 2008):

$$a_w = \left(\frac{n_w}{n_w + i_s n_s}\right) = \left(1 + i_s\frac{n_s}{n_w}\right)^{-1} = \left(1 + \frac{n_{sum}M_w}{\rho_w \frac{\pi}{6}\left(D_{wet}^3 - d_s^3\right)}\right)^{-1} \quad (3)$$

in which d_s is the diameter of the dry particle, n_s and n_w are the amount of substance (number of moles) of solute and of water in the solution, respectively, and n_{sum} is the sum of the different contributing components in the particles, calculated as

$$n_{sum} = \sum_i \frac{\varepsilon_i i_i \rho_i d_s^3}{M_i}\frac{\pi}{6} \quad (4)$$

in which ε_i is the volume fraction of a component i in the dry particle of diameter d_s, i_i is the van't Hoff factor and ρ_i the density of the component, and M_i is the corresponding molecular mass for that particular component. For hygroscopic salts (strong electrolytes) such as ammonium sulfate and sodium chloride the van't Hoff factor is similar (but not identical) to the stoichiometric dissociation number (ν_s), i.e. the number of ions per molecule or formula unit ($\nu_{(NH_4)2SO_4}$ =3, ν_{NaCl} = 2). Deviations between i_s and ν_s can be attributed to solution non-idealities. The van't Hoff factor can be calculated using (see e.g. Kreidenweis et al., 2005; Florence et al., 2011)

$$i_s = \nu_s \phi_s. \quad (5)$$

If the solution is non-ideal, ϕ_s deviates from unity, i.e. ϕ_s represents the molal or practical osmotic coefficient of the solute in aqueous solution.

The hygroscopicity parameter κ is a broadly used parameter for direct comparison of hygroscopicity between H-TDMA and CCNC measurements (Petters and Kreidenweis, 2007), related to a_w as follows:

$$a_w = \left(1 + \kappa\frac{V_s}{V_w}\right)^{-1} = \frac{D_{wet}^3 - d_s^3}{D_{wet}^3 - d_s^3(1-\kappa)}, \quad (6)$$

where V_s and V_w corresponds to the solute volume (assumed as the dry particle volume) and the water volume, respectively. In the same way as n_{sum} above, κ is the total contribution from all volume fractions of components in the particle and is given by a simple mixing rule:

$$\kappa_{sum} = \sum_i \varepsilon_i \kappa_i \quad (7)$$

$$\kappa_i = i_i \times \left(\frac{\rho_i M_w}{\rho_w M_i}\right) \quad (8)$$

and κ can alternatively be calculated from paired s_c–d_s values, derived from CCNC measurements, with the following approximation (valid for $\kappa > 0.2$):

$$\kappa_{CCN} = \left(\frac{4A^3}{27 d_s^3 \ln^2 s_c}\right) \quad (9)$$

$$A = \left(\frac{4\sigma_{sol} M_w}{RT\rho_w}\right). \quad (10)$$

For $0 < \kappa < 0.2$ the contribution of the initial dry aerosol particle volume to the total volume of the droplet is non-negligible and the behaviour approaches that predicted by the Kelvin equation, i.e. expected for an insoluble but wettable particle.

4 Modelling

4.1 CCN activation modelling

As discussed by others (e.g. Khalizov et al., 2009; Tritscher et al., 2011; Henning et al., 2012; Rissler et al., 2012) the non-sphericity and restructuring of the soot particles will introduce a systematic error assessing the volume from measurements of the mobility diameter (d_m). In the κ model the particles are assumed to be spherical. Here, d_m is converted into volume-equivalent diameter (d_{ve}), to account for the non-sphericity of the dry particles when using κ-Köhler theory (d_{ve} is used in a similar way as in Tritscher et al., 2011). The sizes of the dry particles (d_{ve}) as well as the soot and total organic mass fractions (mf_{BC}(APM) and mf_{org}(APM), respectively) in the particles were derived from direct measurements of the relationship between particle mass and mobility diameter, using the DMA-TD-APM set-up (see details in Sect. 2.1). Calculations are performed according to (McMurry et al., 2002)

$$d_{ve} = \sqrt[3]{\frac{6}{\pi}\frac{m}{\rho_{corr}}}, \quad (11)$$

where m is the particle mass and ρ_{corr} is the corrected material density of the particles, assessed from

$$\frac{1}{\rho_{corr}} = \frac{mf_{BC(APM)}}{\rho_{BC}} + \frac{mf_{SOA(APM)}}{\rho_{SOA}} + \frac{mf_{POA(APM)}}{\rho_{POA}}, \quad (12)$$

where mf_{BC}(APM), mf_{SOA}(APM), and mf_{POA}(APM) are the contributing mass fractions in the particles of the different components, approximated as described below.

The initial mass fraction of POA (mf_{POA}(APM)) has been approximated with the measured values of mf_{org}(APM), before the onset of UV. The mass ratio of soot to POA is assumed to be constant for particles of a specific size throughout the experiment. Therefore, after the onset of UV, mf_{POA}(APM) is assumed to decrease at the same rate as mf_{BC}(APM). This assumption of constant proportions between soot and POA is consistent with measurements by the SP-AMS. Hence, after the onset of UV, mf_{POA}(APM) is subtracted from mf_{org}(APM) to calculate the mass fraction of SOA (mf_{SOA}(APM)). Volume fractions (ε_i) for the different components have been calculated from the mass fractions and densities, to be used in the κ-Köhler modelling as well as in calculating ρ_{corr} above.

In this study a high correlation is observed between the volume-equivalent diameter (d_{ve}), the mobility diameter (d_m) and the SOA mass fraction (mf_{SOA}(APM)) in the particle (Supplement, Fig. S2). Hence, by applying a fit to the empirical data, an estimated volume-equivalent diameter ($d_{ve,fit}$) has been derived from d_m and mf_{SOA}(APM) to gain a higher resolution in the κ-Köhler modelling (see equations in Sect. 5.3).

The water activity is calculated from knowledge of the molar masses of the components in the particle. The mean molar mass (M) is a difficult property to measure, as pointed out by Hallquist et al. (2009). In the literature a variety of average molar mass (M) for both SOA ($\sim$ 0.15–0.480 kg mol^{-1}; Hallquist et al., 2009; Kuwata et al., 2013) and POA (0.25–0.7 kg mol^{-1} for lubrication oil; e.g. Stubington et al., 1995) are reported. The difference in molar mass among studies is probably due to different experimental conditions (e.g. combustion conditions, NO_x regime, aerosol loading, oxidants and precursors used). In this study the molar masses have been set to values of 0.2 kg mol^{-1} and 0.4 kg mol^{-1} for SOA and POA, respectively (Table 2). M_{SOA} is a mean value derived from model runs (see Sect. 4.2), while M_{POA} is approximated with the molecular weight of octacosane (C_{28-}, $M = 0.395$ kg mol^{-1}; Lide, 2005) a representative component in lubrication oil.

In the same way, the material densities for POA and SOA is set to constant values of 800 and 1400 kg m^{-3}, respectively – 800 kg m^{-3} is typical for hydrocarbons (Ristimaki et al., 2007). The density for SOA is derived from measurements of the aged particles in this study, in agreement with previously reported densities of anthropogenic SOA formed from *m*-xylene and toluene (e.g. 1330–1480 and 1240–1450 kg m^{-3} respectively; Ng et al., 2007). For the soot particles a primary particle density of 1850 kg m^{-3} is used in the model, in good agreement with previous studies. A density of 1800–2000 kg m^{-3} is often reported for the compacted soot core, e.g. 1840 kg m^{-3} (Choi et al., 1994), 1800 kg m^{-3} (Ristimaki

et al., 2007) and 2000 kg m^{-3} (Park et al., 2003; Cross et al., 2007).

In this study SOA is treated as a water-soluble compound ($i_{SOA} = 1$; Svenningsson et al., 2006) and POA as a water insoluble compound ($i_{POA} = 0$, for example octacosane is not water soluble, Lide, 2005; $\kappa \approx 0$–0.02 for SOA formed from lubrication oil, Lambe et al., 2011). Using the above values for molecular weight, density and van't Hoff factor as input the estimated values of κ_i becomes: $\kappa_{SOA} = 0.1265$ for SOA, $\kappa_{POA} = 0$ for POA and $\kappa_{BC} = 0$ for the soot core, respectively. The calculated κ_{SOA} value is similar as reported in the literature for isoprene-derived secondary organic material particles ($\kappa = 0.12 \pm 0.06$; Kuwata et al., 2013, and references therein), laboratory smog chamber SOA from trimethylbenzene ($\kappa \approx 0.04$–0.15; Jimenez et al., 2009), κ values of SOA formed from *m*-xylene and toluene ($\kappa \approx 0.1$–0.27; Lambe et al., 2011) and photochemically aged diesel soot particles ($\kappa = 0$–0.13; Tritscher et al., 2011).

For fresh POA a κ value below 0.1 is expected, due to the low O : C ratio (< 0.2, not shown) and high M_{POA} of the material, as pointed out by others (Tritscher et al., 2011; Kuwata et al., 2013). If impurities (such as sulfur) are present in the fuel κ values greater than 0.1 may be found (Gysel et al., 2003). However, Tritscher et al. (2011) concluded that the κ value for the fresh emissions (soot + POA) should be close to zero, due to low sulfur content in the fuel used in the study. In this study low-sulfur fuel was used (< 10 ppm) and the AMS detected no particulate sulfate (< 4 ng m^{-3} during 1 min of detection). Therefore, POA is treated as a water-insoluble compound. Due to the insolubility of BC, the soot particle as a whole is treated as water insoluble.

The input parameters for the modelling exercises are thus independently derived and have not been varied to fit the empirical results.

4.2 Modelling of gas-phase chemistry, organic aerosol formation and composition: ADCHAM

In order to better understand the mechanisms responsible for the observed changes in SOA coating, chemical composition and hygroscopic properties and to bring the discussion further, detailed modelling was performed of the gas-phase chemistry, SOA formation and composition during one of the experiments (DEP2, see Table 1). DEP2 was chosen due to the good cover in empirical results of cloud activation properties, mass–mobility relationship and particle chemical composition. For this we used the Aerosol Dynamics, gas- and particle-phase chemistry model for laboratory CHAMber studies (ADCHAM; Roldin et al., 2014). ADCHAM is a model primarily intended to be used to recreate laboratory chamber experiments on SOA. The model explicitly simulates the deposition and re-evaporation of organic compounds from the chamber walls, all fundamental aerosol dynamics processes, detailed gas- and particle-phase chemistry and the mass transfer limited mixing of compounds in the particle phase. It uses the detailed gas phase Master Chemical Mechanism version 3.2 (Jenkin et al., 2003), an aerosol dynamics and particle phase chemistry module and a kinetic multilayer module for diffusion-limited transport of compounds between the gas phase, particle surface and particle bulk phase. In the online Supplement we describe in detail how the ADCHAM model was set up.

5 Results and discussion

5.1 The overall picture

No activation into cloud droplets was observed for the fresh soot particles at supersaturation below 2 %, neither from the diesel exhaust (DEP) nor from the flame soot generator (FSP) experiments (further described in Sect. 5.2). This is in agreement with previous observations, e.g. Tritscher et al. (2011) and Henning et al. (2012). The newly emitted diesel exhaust aerosol shows a carbon mean oxidation state in the range −1.9 to −1.6 (Fig. 2a), obtained from AMS results (where the carbon mean oxidation state ≈ 2 O / C–H / C; Kroll et al., 2011). The results are similar to previous studies (Kroll et al., 2011). Furthermore, the mass spectrum of the newly emitted diesel exhaust aerosol shows an organic (POA) content of mostly hydrocarbon species (Fig. 2b), consistent with diesel exhaust measurements by Canagaratna et al. (2007). An increase in carbon mean oxidation state is visible at the onset of UV exposure (Fig. 2a). At the same time measurements (AMS) as well as modelling (ADCHAM) of the H:C ratio shows a decrease (Supplement, Fig. S4d). The mass spectra of the organic content (POA) of the aerosol emitted from the soot generator are very similar to the mass spectra of the POA from the diesel exhaust aerosol. According to measurements of the chemical composition, inorganic salts do not form during the early stage of the experiments.

The morphology of the fresh emissions from both the diesel vehicle and the flame soot generator has been characterised in detail elsewhere (Rissler et al., 2013). The primary particle diameters are consistent between experiments for the DEP but differing for the FSP, depending on how the generator was operated. In summary, the count median diameter of the primary particle diameter (d_{pp}) in the agglomerates from the diesel vehicle (experiment DEP1-4) was ∼ 28 nm by number, see Table 1. From the flame soot generator agglomerates with two different d_{pp} were generated – agglomerates with a smaller d_{pp} of about 18 nm by number (experiment FSP2) and agglomerates with a larger $d_{pp} \approx 27$ nm by number (FSP1). TEM samples for experiments FSP1 and FSP2 are missing. However, the primary particle diameters have been calculated from the measurements of the particle mass and mobility diameter, according to Rissler et al. (2013). Results from these measurements show that the volume-equivalent diameters (d_{ve}) of FSP1 are closer to the d_{ve} of the DEP (Supplement, Fig. S2 – FSP1 (circles) and DEP1-3

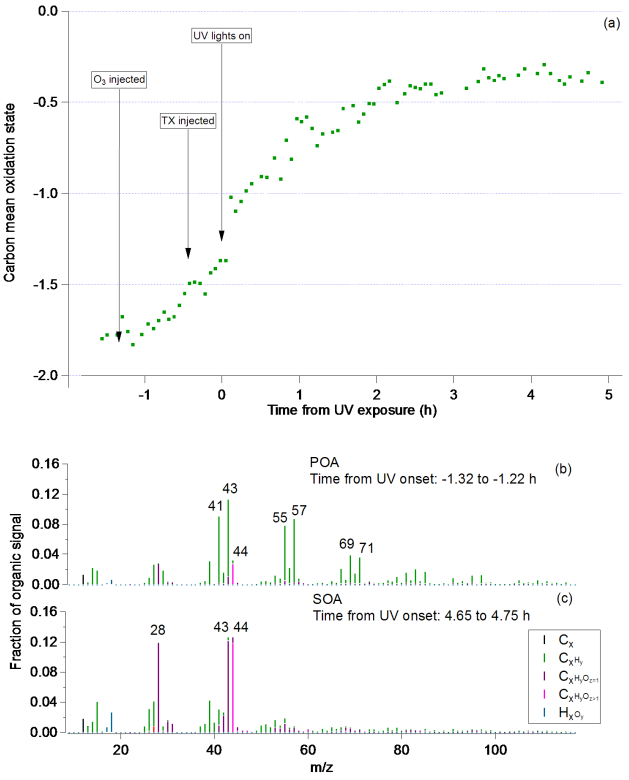

Figure 2. Evolution of the carbon mean oxidation state of the organic material coating the diesel soot **(a)** (carbon mean oxidation state $\approx 2\,\mathrm{O}/\mathrm{C}-\mathrm{H}/\mathrm{C}$; Kroll et al., 2011), during DEP2. Also shown are the high-resolution mass spectra for the POA **(b)** and SOA **(c)**, ~ 1 h before and ~ 5 h after the onset of UV exposure respectively. The characteristic for urban POA is the high amount of hydrocarbons, especially m/z 43 and 57. More oxygenated species, where m/z 44 is dominating over m/z 43, are typical for more rural SOA. Also, the latter show a higher carbon mean oxidation state than the former.

(triangles) fall on the same line), implying that the primary particle diameter (d_{pp}) also is similar for FSP1 and DEP, but different for FSP2. The differences between FSP1 and FSP2 are reflected in the CCN measurements, where FSP1 and DEP require a more similar supersaturation for activation, further discussed in Sect. 5.2. The number size distribution showed a geometric mean mobility diameter (GMD) average for all DEP experiments of ~ 82 nm (with standard deviation, $\sigma_{\mathrm{g}} \approx 1.8$) for the fresh soot aerosols, ranging from 76 to 92 nm ($1.78 < \sigma_{\mathrm{g}} < 1.89$) between experiments. The fresh aerosols from experiments FSP1 and FSP2 showed a GMD of ~ 117 nm ($\sigma_{\mathrm{g}} \approx 1.63$) and ~ 79 nm ($\sigma_{\mathrm{g}} \approx 1.88$), respectively. The parameters (GMD and σ_{g}) were determined from the fitted lognormal number size distributions. Primary particle diameters (d_{pp}) from calculations and TEM picture analysis as well as selected sizes (d_{m}) for the CCN measurements for the different experiments are listed in Table 1.

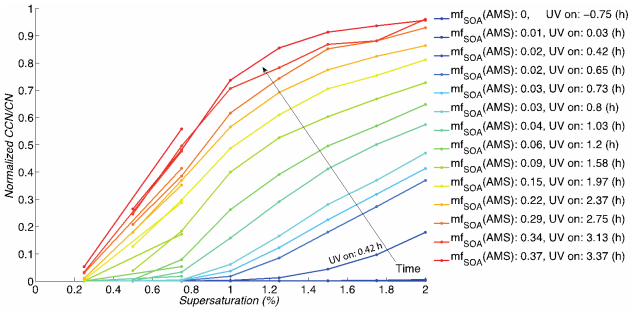

Figure 3. The evolution of the activation properties for the whole aerosol during the ageing event of experiment DEP3. Measurements from two CCNCs are overlapping in the range $0.25 <$ supersaturation < 0.75 %, thereby are two lines visible for the low supersaturations. Before and just after the onset of UV exposure (UV on $= -0.75$ and 0.03 h respectively) almost no particles (< 1 %) are activated (dark blue) and the SOA mass ratio ($\mathrm{mf_{SOA}}$) is close to zero. $\mathrm{mf_{SOA}}$(AMS) is estimated from measurements from the SP-AMS. As the soot particle acquires more organic material ($\mathrm{mf_{SOA}}$ increase) the CCN properties improve. By the end of the experiment (UV on $= 3.37$ h) all particles are activated (dark red) and $\mathrm{mf_{SOA}} \approx 0.4$.

At the onset of UV exposure, an immediate (within 5 min) enhancement of the activation properties of the coated soot cores is seen. Typically, the first full supersaturation spectra were measured within the first 10–15 min after onset of UV exposure, for the particle size-resolved aerosol (see Sect. 5.2 for details). In the early stage of the experiments, a mobility diameter (d_{m}) of 150 nm was selected, in most experiments. The selected size was based on the knowledge that particles of a smaller d_{m} were not activated in the beginning of the experiments and particles with larger d_{m} were too few in number. Furthermore, focusing on one size improved the time resolution of the measurements substantially. During one experiment (DEP3, Fig. 3) the whole aerosol was measured continuously, without any size selection upstream of the CCNC. In the beginning of this experiment a small number fraction of particles of the whole aerosol (< 1 %) activates at high supersaturation (> 2 %). This was the only experiment showing this early activation, which could either be activation of exhaust aerosol or impurities. As the aerosol ages, the particles become better CCN and by the end of the experiment almost the whole aerosol is activated at high supersaturations (> 1.6 %) (Fig. 3).

The minimum d_{m} that was able to activate at a certain supersaturation, at a certain SOA mass fraction ($\mathrm{mf_{SOA}}$(AMS)), was retrieved by integrating number size distributions from larger to smaller sizes (Fig. 4). Here, the SOA mass fraction ($\mathrm{mf_{SOA}}$(AMS)) is estimated from measurements from the SP-AMS, in the same way as the SOA mass fraction ($\mathrm{mf_{SOA}}$(APM)) is estimated from the APM measurements, but for the whole size distribution (information on the procedure to derive the masses of BC and organic material from

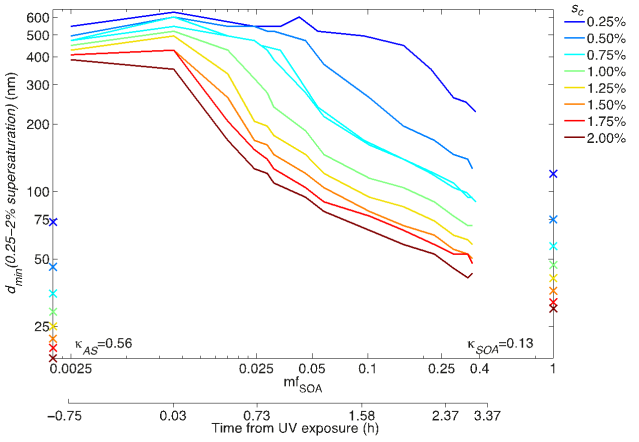

Figure 4. The minimum mobility diameter ($d_{m,min}$) required for activation of the diesel exhaust particles (DEP3) at different supersaturations (supersaturation; colour coded) with respect to the SOA mass fraction (mf_{SOA}(AMS)), for the whole aerosol measured by SP-AMS. As the mf_{SOA}(AMS) increases, the activation properties of the diesel exhaust aerosol particles improve, i.e. there is an increase of activated particles of smaller sizes for a certain supersaturation. Also shown are the theoretical values for ammonium sulfate particles (AS, $\kappa_{AS} \approx 0.56$, organic fraction = 0) and organic particles ($\kappa_{SOA} \approx 0.13$, organic fraction = 1). Note that before and just after the UV exposure only about < 1 % of the particles are activated.

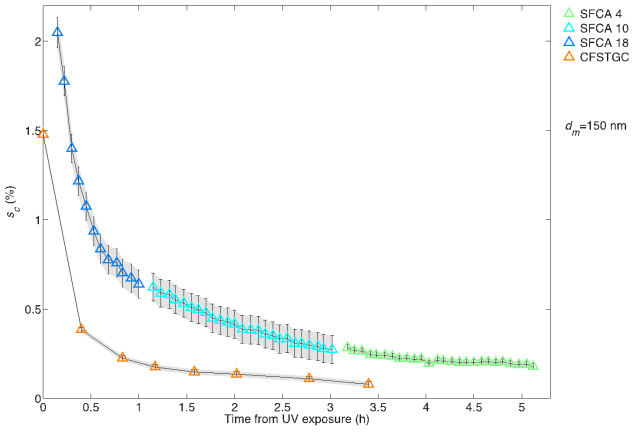

Figure 5. Comparison of the two measurement techniques continuous-flow streamwise thermal-gradient CCNC (CFSTGC, orange) and Scanning Flow CCN Analysis (SFCA, blue, red and green) with error bars (black) representing 95 % confidence intervals, from experiments DEP1 and DEP2 respectively. The change in s_c over time for diesel exhaust particles is captured in both experiments, though with a better resolution while using SFCA. A slower decrease of s_c is seen in DEP2 (SFCA) due to altered experimental conditions, with a slower ageing process. During DEP2 the temperature gradient (ΔT) was changed three times (4 K, blue; 10 K, red; and 18 K, green). Note that the first measurement point using CFSTGC was possible due to letting the experiment scan past a constant supersaturation and d_m (see Sect. 2.1 for more information).

SP-AMS data is found in the Supplement). Hence, size distribution measurements, from the SMPS, along with the change in SOA mass fraction, derived from the SP-AMS, are linked to the activation properties measured by the CCNC. For example, at the onset of UV exposure, if the particles are exposed to a supersaturation of 1 %, a minimum d_m of 480 nm is required to activate 0.2 ‰ exhaust particles (Figs. 3 and 4). The mf_{SOA}(AMS) has increased slightly from 0 to ∼ 0.01 at this point. As the exhaust particles acquire more SOA they become better CCN. By the end of DEP3 the mf_{SOA}(AMS) is about 0.4 and the minimum d_m has decreased to about 60 nm for a supersaturation of 1 %.

The observation of an immediate change in activation at the onset of UV exposure is consistent in all experiments, independent of amounts of added precursors, oxidants and soot particle source. Due to the new way of operating the CCNC, using scanning flow (SFCA) with a higher supersaturation and time resolution, it was possible to cover the development of the activation properties more thoroughly than ever done before (Figs. 5–7, "s_c"). Hence, it was possible to capture both the onset of activation, covering the very first changes of the particles becoming better CCN, as well as following the evolution of the particles.

The evolution of a decreasing s_c, along with an increasing SOA mass fraction (mf_{SOA}(APM)) coating the soot cores and a change in volume-equivalent diameter is illustrated in Fig. 6 (DEP2). The decline of s_c continues throughout the ageing process, although the effect is more prominent at the beginning of the process. For the mf_{SOA}(APM) the trend mirrors the s_c, with a higher increase in mass fraction at the beginning which levels out by the end. The rate of decreasing s_c and increase of coating mf_{SOA}(APM) differ between experiments (compare Figs. 6 and 7), i.e. the rates are dependent on amount of SOA precursors and ozone added, and NO_x levels. The time of photochemical ageing in the smog chamber, until the soot particles become CCN active at a supersaturation of 0.2 % (equivalent to the supersaturation in a stratocumulus cloud), range from 1.5 to > 4.5 h. With respect to organic condensational growth this corresponds to an atmospheric ageing time at the mid-latitudes of between 4 h and a few days (for details see Supplement). However, in the atmosphere other compounds, such as biogenic organics and inorganics, are present which also will affect the hygroscopicity and the lifetime of the soot particles, hence the calculated atmospheric ageing time is an approximation.

5.2 Detailed picture

In general, cloud droplet formation ability of aerosol particles can be described as a function of the number of dissolved molecules and ions in the activating droplet, parameterised by for example the κ value. In the case of particles dominated by soot, the volume occupied by insoluble material

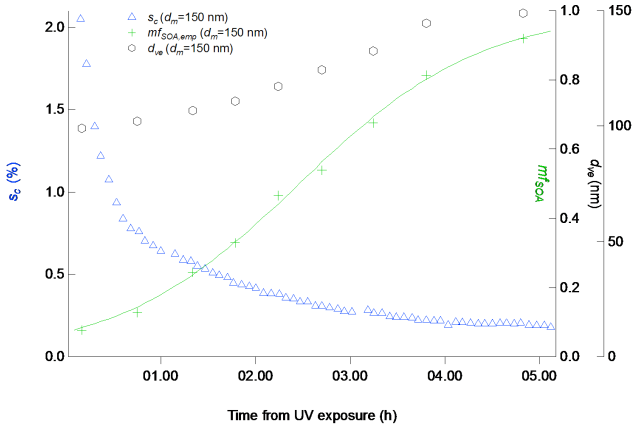

Figure 6. Changes in s_c (blue), mf_{SOA} (green markers, empirical; green line, fit) and d_{ve} (black) over time for diesel exhaust particles, during experiment DEP2. No activation of particles was seen before the onset of UV.

influences the Kelvin effect and therefore has to be taken into account. In present experiments, the time-dependent changes of activation properties of the coated soot cores are summarised by four factors: (I) particle organic fraction; (II) type of organic coating (POA or SOA); (III) particle size; and (IV) morphology. Here, the results with respect to each of these factors will be discussed.

(I) The ability of the soot cores to act as CCN increases with increasing amount of organic coating material, i.e. increases in SOA mass fraction (mf_{SOA}(APM)) (Figs. 6 and 7). At the end of the ageing process, when the SOA mass fraction makes up most of the particles ($mf_{SOA}(APM) \geq 0.7$, size dependent), the s_c levels out. In all experiments, all measured sizes show the same trend. The condensation rate of SOA was different in different experiments. However, independent of the rate, s_c is more or less the same for a chosen size with a certain mf_{SOA}(APM).

(II) No activation was observed in the early stage of the ageing process, i.e. before UV exposure, although an increase is visible in carbon mean oxidation state (Fig. 2a). At this stage the soot core makes up most of the particle mass ($mf_{BC}(APM) \sim 0.9$), and the remaining fraction is dominated by POA. The mass spectral signature measured by the AMS corresponds well with hydrocarbon like OA (HOA) commonly found in urban environments (Jimenez et al., 2009) and previous diesel exhaust emission (Canagaratna et al., 2007) studies of POA (an example from DEP2 is shown in Fig. 2b). POA originates from the combustion process (presumably from lubrication oil) and even as the POA reacts (change in carbon mean oxidation state, Fig. 2a) before the onset of UV exposure it is not hygroscopic enough to suppress the s_c below 2 %. According to simulations with the ADCHAM model (Roldin et al., 2014, Sect. 4.2) no SOA is formed before the UV light is turned on, and according to the simulations the concentrations of ozone, hydroxyl radicals (OH) and nitrate radicals (NO_3) at this stage are insignificant (see Fig. S3 in the Supplement). Also, no detectable particle mass increase or fundamental changes in the mass spectra are observed before the onset of UV radiation, other than a slight increase in m/z 44 due to CO_2^+. Hence, it is unlikely that any substantial SOA formation is taking place during dark conditions, before the onset of UV exposure (DSOA in Fig. 8). Instead, the increase in carbon mean oxidation state can be explained by heterogeneous oxidation of POA by NO_2 at the surface of the soot core (illustrated in Fig. 8 as OPOA). Such reactions have previously primarily been studied because of their potential importance for HONO formation in the atmosphere (e.g. Arens et al., 2001; Han et al., 2013). Using ATR-IR spectra Han et al. (2013) observed a great increase in several absorbance bands associated with nitro (R–NO_2) and nitrate (R–O–NO_2) organic functional groups, after NO_2 exposure. However, in our experiments the altered chemical composition of the organic coating material, i.e. a change in carbon mean oxidation state, does not affect the activation properties of the particles at supersaturations $\sim$2 %. As concluded by Tritscher et al. (2011) it cannot be ruled out that the hydrophobicity of the particles' surfaces could be a hindering effect of the particles to act as CCN. All experiments show an initial O : C ratio < 0.2, which according to Kuwata et al. (2013) classifies non-CCN-active compounds. Also, lubrication oil (for example, octacosane or C_{28}), which POA originates from, is not water soluble (Lide, 2005). In general it should be pointed out that the organic mass fraction (mf_{org}(APM)) is low throughout the period before UV exposure. The initial total organic aerosol (OA) fraction is 2–8 % and just after the onset of UV radiation (up to 30 min in some experiments) it is still low (typically < 9 %), i.e. the amount of formed oxidised material in the early stage of experiments is very small compared to the SOA fraction of the aged soot in this study.

As mentioned in Sect. 5.1, the first enhancement in hygroscopicity of the particles is observed when the exhaust aerosol and precursors are subjected to UV. Weingartner et al. (1997, and references therein) proposed that this change could be attributed to e.g. photolysis of Polycyclic aromatic hydrocarbon (PAH), or an oxidation of the particle surface from photochemically produced hydroxyl radicals (OH), or condensation of photochemically produced compounds. At the onset of UV exposure there is often (but not always) a detectable increase in the organonitrate (R–ONO_2) level in the chamber. Also, more oxidised organic compounds

are produced (increase in carbon mean oxidation state, illustrated in Fig. 2a). Condensation of organonitrates and other oxidised organic compounds, at the soot surface, would improve the hygroscopicity of the particle (illustrated in Fig. 8). Another possibility of the change in CCN properties at the onset of UV is oxidation of POA by OH or ozone. Probably both mechanisms take place and contribute to improved CCN activity.

According to the ADCHAM model simulations of the DEP2 experiment, it takes approximately 1 hour during this experiment before oxidation products of the added precursors *m*-xylene or toluene start to contribute to the SOA formation. Instead, the initial SOA formation, after the onset of UV exposure, is likely to be condensation of low-volatile organic compounds formed when OH reacts with intermediate volatility organic compounds (IVOCs; Donahue et al., 2009) present in the diesel exhausts. Naphthalene, alkylnaphthalenes and other PAHs are present in diesel exhausts (although at lower levels than light aromatic compounds and alkanes) (Schauer et al., 1999). Still, because of their high reactivity towards OH and large fraction of low-volatile oxidation products (high SOA yields), they may dominate the initial SOA formation in fresh diesel exhausts (see e.g. Chan et al., 2009). However, with the best estimate of the PAH (naphthalene) concentrations in the chamber, the ADCHAM model still substantially underestimates the initial SOA formation (Supplement).

During the following hours of experiment s_c is declining, as the amount of condensed organics increases. By the end of the ageing process, the organic coating consists mostly of oxygenated compounds with an m/z signature similar to the semi-volatile oxygenated organic aerosol factor commonly representing relatively fresh SOA in the atmosphere (Fig. 2c). Also, the carbon mean oxidation state is about -0.4 (illustrated in Fig. 2a), in the range of what is reported for alkane/alkene photooxidised SOA (Kroll et al., 2011). According to our ADCHAM model simulations of the DEP2 experiment, by the end of the experiment more than 80 % of the SOA mass can be attributed to the oxidation products from the added SOA precursors *m*-xylene and toluene (Fig. S5 in the Supplement). The change in composition of the organic coating into more oxygenated species is more pronounced in the beginning of the ageing process when the POA fraction of OA is still substantial. For example, the carbon mean oxidation state drastically increases in the beginning and then flattens out towards the end (illustrated in Fig. 2a).

(III) A size dependency is evident for both the activation properties as well as for the condensation of organic material. For particles of a specific mf_{SOA}(APM), the smaller particles require a higher supersaturation for activation than the larger ones. This is mainly explained by

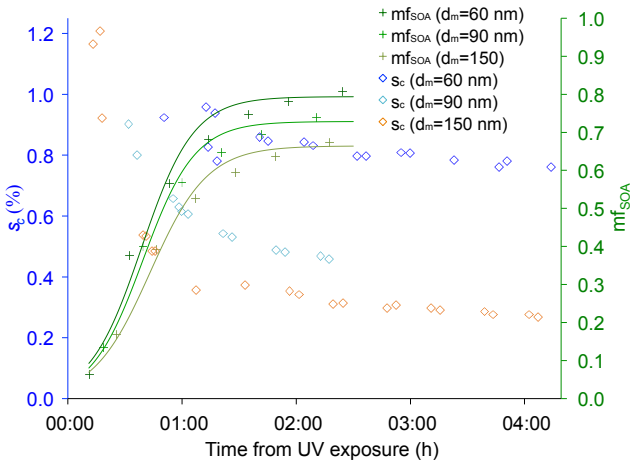

Figure 7. Decreasing critical supersaturation (s_c, blue) and increasing mf_{SOA} (green markers, empirical; green line, fit) for three different mobility diameters ($d_m = 60$, 90, and 150 nm) from measurements of flame soot generator particles over time, during experiment FSP2.

the fewer amounts of water-soluble ions or molecules and thus larger Kelvin effect, which is more pronounced for particles with higher curvature. However, smaller particles are more efficient in relative mass acquisition by SOA condensation (Fig. 7), as pointed out by Tritscher et al. (2011). They found that small particles show the highest hygroscopic growth, although a more efficient acquisition of SOA does not lower the s_c to a degree where it would compensate for a smaller particle size (Fig. 7). It should be pointed out that the size dependence of mf_{SOA}(APM) at a given time is much smaller than that predicted for spherical particles according to transition regime mass transfer models. This is a direct consequence of the highly agglomerated particle morphology (Pagels et al., 2009).

(IV) Fresh soot and particles dominated by soot have an agglomerate structure (Fig. 8), implying that the particle volume is smaller than expected for spherical particles. A restructuring of the agglomerated soot particles is seen during ageing (Fig. 9a–c), in agreement with previous reported work (e.g. Weingartner et al., 1997; Tritscher et al., 2011). Tritscher et al. (2011) argue that shape effects are the main reason for the absence of CCN activation of the fresh emissions. Another possibility is that the acquisition of water-soluble material is not evenly distributed around the soot core, leading to specific activation sites (Fig. 9a). If most of the particles' soluble material is excluded from the droplet at activation (Fig. 9a, solid, blue lines), due to formation of several smaller separate droplets, the critical supersaturation will be higher than expected assuming that all soluble material is in the same droplet and

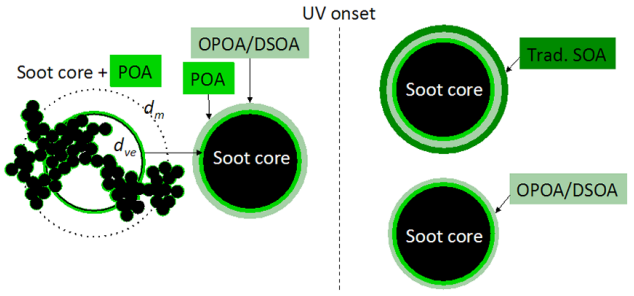

Figure 8. A conceptual model illustrating different processes which might affect the activation properties of the soot particles in the early stage of ageing. Here, POA is evenly distributed over the agglomerate. The volume-equivalent diameter is used to account for the non-sphericity of the particles. In dark conditions (before the onset of UV radiation) POA on the soot surface might be oxidised, i.e. oxidised primary organic aerosol (OPOA). Another possibility is that gas-to-particle conversion processes may occur, i.e. secondary organic aerosol produced in dark conditions (DSOA) condenses onto the soot particles. At the onset of UV the organic material on the soot surface (OPOA and/or DSOA) might be further oxidised, and/or condensation of oxidised material (traditional SOA), and/or condensation of small amounts of organonitrates transforms the particles from non-activating into activating CCN, at ~2 % supersaturation.

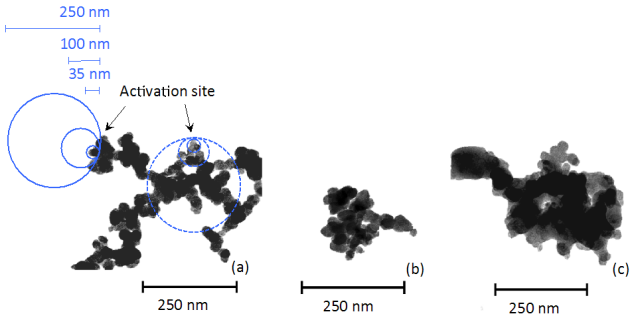

Figure 9. TEM pictures of diesel exhaust particles (DEP1): a fresh diesel exhaust particle **(a)**, after 1 h **(b)** and 4 h of ageing in the chamber **(c)**. In **(a)** an activation site excluding most of the particles' soluble material in the droplet at activation is illustrated (solid, blue circles), as well as a site with more material included (dashed, blue circles), for the diameters 35, 100, and 250 nm.

involved in the activation. In contrast, if droplet growth starts at different sites successively incorporating more and more of the particle and growing to form one single droplet (one of these sites is illustrated in Fig. 9a, dashed, blue lines) all soluble material in the particle is involved in the activation.

The particles become more compact and spherical-like with increasing amount of organic (SOA) coating material (Fig. 9c). This is due to a combination of two effects: SOA material filling the void spaces (Nakao et al., 2011) and restructuring of the agglomerates. The restructuring is due to condensation of organic (SOA) material onto the soot particles in the smog chamber. Additionally, condensing water in the CCNC may enhance the effect of restructuring. The changed morphology due to for example SOA condensation is illustrated in Fig. 6 (increase in d_{ve} during experiment DEP2), Fig. 9 (TEM pictures of processed DEP) and Fig. 10 (s_c decrease with increasing d_{ve}, experiments DEP2, DEP4 and FSP1, FSP2). The fresh soot particles show a size-dependent morphology, with higher dynamic shape factor values for the larger particles than for the smaller ones. The dynamic shape factor ($\chi = (d_m/d_{ve})^*(C_c(d_{ve}))/(C_c(d_m))$; DeCarlo et al., 2004) typically increases with increasing mobility size and with decreasing primary particle size. It varied between 1.7 and 2.5 for the freshly emitted highly agglomerated soot particles, for all sizes measured here. At the end of the experiments the particles are more spherical-like, with a shape factor close to 1. As the particles grow by coagulation in the combustion process they develop larger branches with a highly agglomerated structure. When larger, more branched particles are subjected to the ageing process, they will experience a more pronounced restructuring. Weingartner et al. (1997) found that the DEP exhibit a smaller restructuring combined with condensational growth than the soot aggregates from the soot generator. This might be an effect of the primary particle size. More-branched (less dense) aggregates are formed when smaller primary particles are present in the combustion process from the soot generator (FSP2). Hence, the FSP with the smaller d_{pp} (by number) $\approx$ 18 nm are able to restructure to a larger extent. The empirically derived d_{ve} are smaller for the agglomerates with a smaller d_{pp} (FSP2) compared to the agglomerates with a larger d_{pp} (by number) of 28 nm ($\approx$ FSP1 and all DEP experiments), at the same mf_{SOA}(APM). Although the activation properties show very similar results for the two different kinds of soot, there is a slight difference. Particles with the smallest d_{pp} (FSP2) are slightly better CCN for a given d_{ve} (compare diamonds with circles and/or triangles, $d_m = 150$ nm, in Fig. 10). These particles (FSP2) are probably activating at a lower supersaturation due to a smaller mass of soot for a given d_m and hence a larger SOA mass, than a particle with larger d_{pp} (DEP and FSP1) for a certain d_{ve}. However, for a given mf_{SOA}(APM) the same particles (FSP2) need a slightly higher supersaturation for activation than the soot agglomerates with larger primary particles (compare diamonds with circles and/or triangles, $d_m = 150$ nm, in Fig. 11). For the same mf_{SOA}(APM), a particle with larger d_{pp} will activate at a lower supersaturation due to a larger size of the agglomerate (d_{ve}), thereby also containing more water-soluble molecules than a particle with smaller d_{pp}.

5.3 Modelled vs. empirical results

Simple Köhler theory as well as κ-Köhler theory was used in this study, showing the same results (described in Sect. 3). Therefore, the κ-Köhler model represents results from both

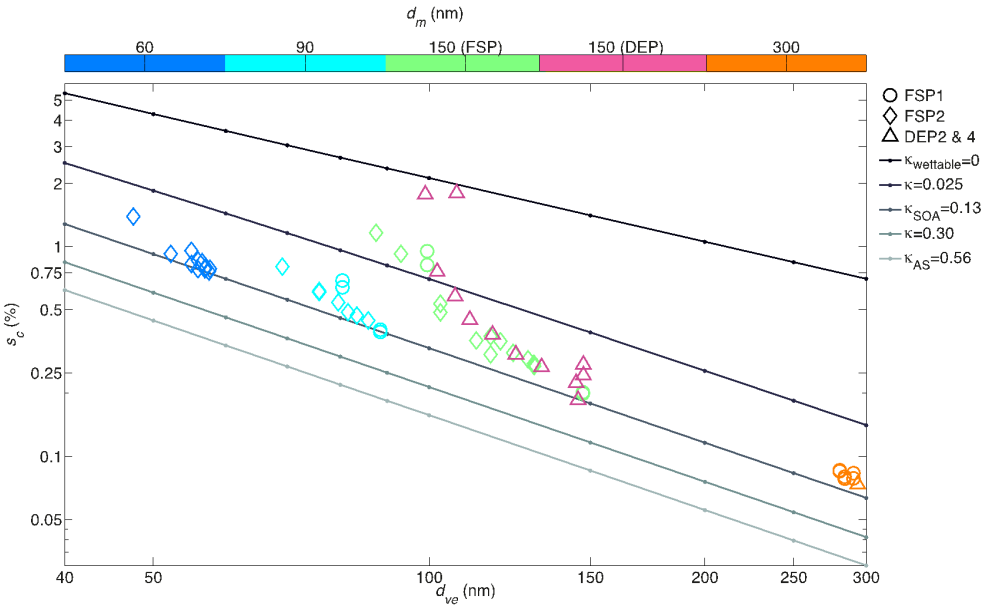

Figure 10. Empirical s_c for different volume-equivalent diameters (d_{ve}), size-selected according to their mobility diameter (d_m; colour coded) in comparison with calculated values of s_c from κ-Köhler theory (greyscaling). Modelled values ranges from insoluble but wettable particles ($\kappa_{wettable} = 0$, black line) to AS particles ($\kappa_{AS} \approx 0.56$, lightest grey) in the size range 40–300 nm. Also plotted are modelled values for the κ value derived for the SOA appearing at the end of the experiments in this study ($\kappa_{SOA} \approx 0.13$). Triangles denote coated diesel soot particles (DEP1, 2 and 4). Coated soot generator particles are represented by diamonds (FSP2) and circles (FSP1), differentiated due to their different primary particle sizes.

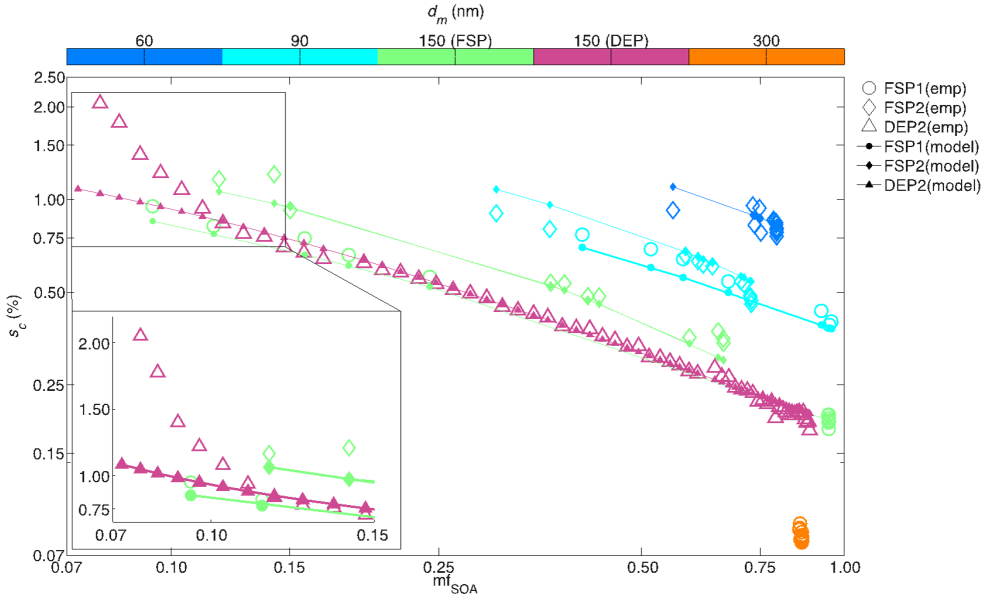

Figure 11. Measured critical supersaturation (s_c) by estimated mass fraction SOA (mf_{SOA}), for experiments FSP1 (circles), FSP2 (diamonds) and DEP2 (triangles). Also shown are κ-Köhler modelled results using $d_{ve,fit}$ as input for d_s (filled markers/lines). The measured mobility diameter of the particles are colour coded, separating only the FSP from DEP measurements for $d_m = 150$ nm ($d_m = 60$ nm, dark blue; $d_m = 90$ nm, light blue; $d_{m,FSP} = 150$ nm, green; $d_{m,DEP} = 150$ nm, pink; $d_m = 300$ nm, orange). The measurements are well represented by the model for $mf_{SOA} > 0.12$. For lower organic fraction the particle properties are hindering the activation into cloud droplets, i.e. a higher supersaturation is needed for activation. Also, the model is not as representative for FSP2, $d_m = 90$ and 150 nm (green diamonds), as for the other experiments.

these models. To improve the performance of the κ-Köhler model, the input parameters have been tested as follows (Fig. 12). Firstly, a model taking only the Kelvin effect into account was used. In this model the Raoult term is neglected by setting $i_{SOA} = 0$ and the dry diameter (d_s) of the particle is equal to the measured volume-equivalent diameter ($d_{ve,measured}$). The particles are assumed to be insoluble but wettable, hence the model is named Wettable. Secondly, both the Kelvin effect and the chemical composition was taken into account, but neglecting the shape effect (i.e. d_s equals the mobility diameter, d_m). Hence, the model is called κ-Köhler (d_m). In the third model, κ-Köhler ($d_{ve,\,measured}$), both the chemical composition, size and shape are accounted for (discussed in more detail further down). As input parameter for d_s the volume-equivalent diameter (denoted as $d_{ve,measured}$) is used, estimated from the measurements of the mass–mobility relationship (DMA-TD-APM). For the fourth model, d_s is exchanged by the volume-equivalent diameter (d_{ve}) derived from an empirical fit function with input parameters of the mobility diameter (d_m) and mass fraction SOA (mf_{SOA}(APM)), denoted as $d_{ve,fit}$ (Eqs. (13) and (14) below, Fig. S2 Supplement). This model is called κ-Köhler ($d_{ve,\,fit}$) and uses an approximation of the volume-equivalent diameter, performed to gain better time resolution of the modelled results for comparison with empirical results (Figs. S2 and S7a–b in the Supplement).

In the model, the porosity and structure of the coated soot particles as well as the size is partly represented by the number of water-soluble molecules (Raoult's law) and partly by the effect of surface curvature of the solution droplet (the Kelvin effect). The volume-equivalent diameter (d_{ve}) accounts for the change in morphology in the model, and can for a DEP with a primary particle diameter (d_{pp}) of ~ 28 nm, from a Euro II vehicle be approximated by (in nm) (Supplement, Fig. S2)

$$d_{ve,fit,DEP} = (0.540897 \times mf_{SOA} + 0.414766) \times d_m - 24.9877 \times mf_{SOA} + 31.53536, \quad (13)$$

and d_{ve} for a flame soot generator particle (FSP) with a primary particle diameter (d_{pp}) of ~ 18 nm, can be approximated by

$$d_{ve,fit,FSP} = (0.358919 \times mf_{SOA} + 0.490475) \times d_m + 0.764891 \times mf_{SOA} + 11.8527. \quad (14)$$

The mass–mobility relationship and d_{pp} for the diesel soot investigated here is similar to a number of emission studies in the literature (e.g. Park et al., 2003; Maricq and Ning, 2004; Rissler et al., 2013) and the parameterisation may thus be of relevance for diesel exhaust in general. As discussed in Sect. 5.2, the primary particle size of the soot might influence the activation properties. This is partly accounted for by d_{ve} in the model (Fig. 11, FSP2 – diamonds compared to lines), i.e. d_{ve} is smaller for smaller d_{pp} at a given d_m.

The κ-Köhler ($d_{ve,\,measured}$) and κ-Köhler ($d_{ve,\,fit}$) models capture the evolution of the decreasing s_c well, except at the beginning of the ageing process when s_c is underestimated (Fig. 12, turquoise and orange lines, respectively). When the measured mobility diameter is used as input for d_s in the model, κ-Köhler (d_m), the results deviate far from experimental results (Fig. 12, pink line). Only at the end of the ageing process, when the particles are more spherical-like and $d_m \approx d_{ve}$, does the κ-Köhler (d_m) model agree with the empirical results (Fig. 12, pink line vs. blue triangles). In the early stage of the experiments the Wettable model best explains the observed s_c (Fig. 12, green line). Hence, the slightly coated soot particles activate at a higher supersaturation than expected, with the assumption that the organic fraction is SOA with a $\kappa = 0.13$. However, the agreement between Wettable model and the empirical results in the beginning of the experiments might be a misleading coincidence. Activation was clearly occurring and visible in the CCNC at the onset of UV radiation, though measurements of whole activation steps were not possible above 2 % supersaturation. There are many processes and possibilities to explain the changed behaviour of the soot particles, from non-activating into activating CCN, as discussed in Sect. 5.2 (Fig. 8).

The deviation between modelled (κ-Köhler ($d_{ve,\,measured}$) and κ-Köhler ($d_{ve,\,fit}$)) and empirical results in the early ageing process (mf_{SOA}(APM) < 0.12) might be due to hindering shape effects (Tritscher et al., 2011) or possibly only parts of the soot particle serve as activation sites, due to the highly agglomerated structure (Figs. 9a and S7a in the Supplement). If activation sites were considered, the critical diameter corresponding to activation would be much smaller than the diameter of the whole particle (either d_{ve} or d_m is used in the model). A plausible range of d_s would be 30–50 nm, and then the activation diameter would be ~ 100 nm (the same as the volume-equivalent diameter in the beginning of the ageing process). In any case this effect would possibly be more pronounced for the larger particles.

Another possibility (to explain the deviation between modelled and empirical results, for mf_{SOA}(APM) < 0.12) would be a transformation of the hydrophobic organic material to a semi-hydrophilic or wettable material. As suggested by others (Bilde and Svenningsson, 2004; Petters and Kreidenweis, 2008; Kuwata et al., 2013), knowledge about the solubility of the particle material as well as about the particle phase can be important parameters when interpreting experimental data and modelling. Petters and Kreidenweis (2008) argue that the s_c of certain mixtures and solubilities are more sensitive to dry particle diameter and also noticeably affected by small amounts of moderately soluble and hygroscopic compounds. Kuwata et al. (2013) suggested that organic compounds acting as CCN could be divided into three different regimes, depending on the O : C ratio of the material. They found that for the insoluble regime there is no activation into cloud droplets (O : C < 0.2), $\kappa = 0$. Compounds that are highly CCN active are in the highly soluble regime

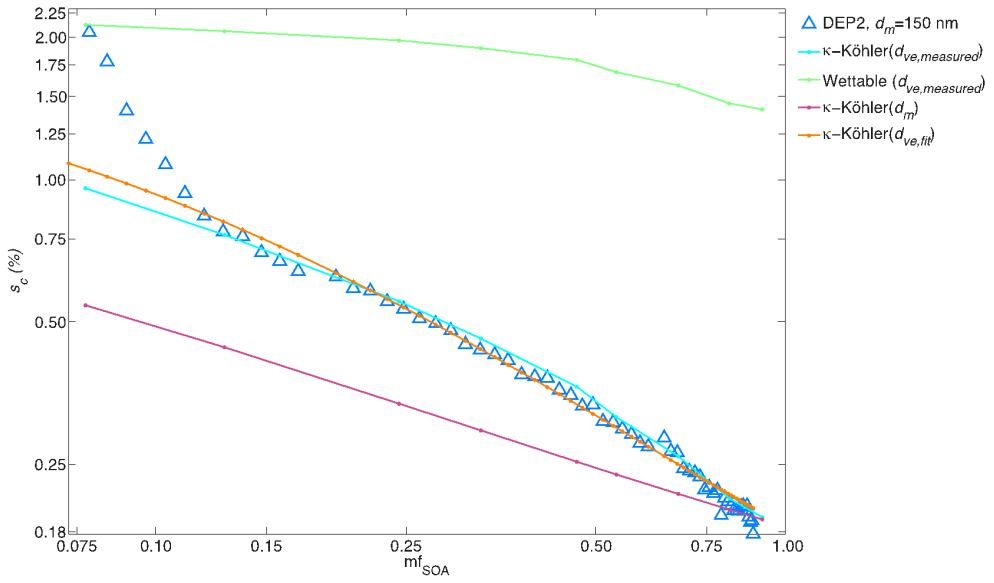

Figure 12. Empirical (blue triangles) vs. modelled (lines) results for experiment DEP2. Four different models are compared: (1) Wettable, taking only the Kelvin effect into account (i.e. $i_{SOA} = 0$) and the dry diameter of the particle (d_s) equals the measured volume-equivalent diameter ($d_{ve,measured}$); (2) κ-Köhler(d_m), accounts for the chemical composition but neglects the shape effect (i.e. d_s equals the mobility diameter, d_m); (3) in κ-Köhler ($d_{ve,measured}$) both the chemical composition and shape effects are accounted for, and $d_s = d_{ve,measured}$; and (4) for the model κ-Köhler ($d_{ve,fit}$) the particle diameter has been calculated by a fit function of $d_{ve,measured}$ and mf_{SOA} (Eqs. 13, 14).

with a $\kappa > 0.1$ (O : C > 0.6). In between (0.2 < O : C < 0.6), most compounds are in the slightly soluble regime with low κ values. Kuwata et al. (2013) also derived a modified κ-Köhler equation, accounting for sparingly soluble compounds. The discrepancy in this study between model and empirical results in the early stage of ageing, when the amount of organic material in the particle and volume of water in the droplet is small (mf_{SOA}(APM) < 0.12, water volume < 50 % of the droplet), could possibly be explained by limitations in solubility (Fig. 12). The investigation and modelling of semi-hygroscopic material to explain the diverging results is not within the scope of this study, but should be a future focus.

At the beginning of the experiments (before the onset of UV exposure) only POA (and/or processed/transformed POA) is assumed to constitute the organic fraction, consistent with the absence of CCN activation at ∼ 2 %. Neither POA nor soot is considered soluble ($\kappa = 0$) in this study (as discussed before) and therefore no activation of freshly emitted particles is visible. At the onset of UV exposure a small quantity of SOA is produced, reflected in the measurements as an immediate change of the particles into becoming better CCN. Also, the mf_{SOA}(APM) was not negligible even if the organic material was only slightly hydrophilic, i.e. water-soluble molecules were probably present at this point. The organic material in the early ageing process is probably either oxidised POA (heterogeneously before the onset of UV, or by OH and/or ozone just after the onset of UV) or SOA formed from condensation of low-volatile organic compounds (probably naphthalene) in the diesel exhaust (discussed in Sect. 5.2). By the end of the ageing process, the formation of SOA from *m*-xylene and toluene is dominating. Either way, the assumptions made for the κ-Köhler modelling in this study are too simple to explain the activation of the slightly coated soot particles (mf_{SOA}(APM) < 0.12). Either the POA (just after UV onset) should be treated as slightly soluble or SOA should be treated as less soluble.

As the ageing proceeds, more SOA condenses onto the particles. The SOA is considered hydrophilic in the model ($\kappa_{SOA} = 0.13$), which will enhance the ability of the soot particles to activate. κ values for ambient particles show high variation depending on content assumed in calculations and instrument used for observations, e.g. $\kappa = 0.04$–0.47 over the American continent (Shinozuka et al., 2009), 0.16–0.46 in Germany (Wu et al., 2013), 0.22 for the oxygenated organic component (Chang et al., 2010) and 0.10–0.20 for Amazonian background aerosol (Rissler et al., 2004; Gunthe et al., 2009). An average κ value of ∼ 0.3 has been observed for many continental locations (e.g. Andreae and Rosenfeld, 2008; Pöschl et al., 2009; Shinozuka et al., 2009; Rose et al., 2010; Hersey et al., 2013). The lower range of κ values in the literature corresponds to a higher content of organics, while the higher values correspond to less organics and a higher content of salts. The low value of κ_{SOA} (= 0.13) in this study compared to urban aerosol hygroscopicity ($\kappa \approx 0.3$) could be attributed to the lack of salts, which are not as present in the chamber experiments as in the atmosphere.

However, the calculated $\kappa_{sum}(=\varepsilon \times \kappa_{SOA})$ is in good agreement with κ_{CCN} (derived from the CCN measurements) for all experiments (Supplement, Fig. S7b). In the literature, κ values for SOA formed from lubrication oil ($\kappa \approx 0$–0.02; Lambe et al., 2011) are in the same range as κ_{sum} and κ_{CCN} at the beginning of the ageing process. By the end of the ageing process κ_{sum} and κ_{CCN} are more similar to κ values of SOA formed from *m*-xylene and toluene ($\kappa \approx 0.1$–0.27; Lambe et al., 2011). κ_{sum} is in the same range as κ values from previous chamber studies of diesel exhaust ($\kappa = 0$–0.13; Tritscher et al., 2011). κ_{CCN} and κ_{sum} deviate the most for the smallest and highest κ values (Fig. S7b, Supplement). Calculations of κ_{CCN} are more uncertain at the beginning of the ageing process, when the κ values are low. κ_{SOA} on the other hand shows larger uncertainties at the end of the ageing process, due to uncertainties in fitted $mf_{SOA}(APM)$ values. As $mf_{SOA}(APM)$ increases, s_c decreases, in agreement with the models (κ-Köhler ($d_{ve,\,measured}$) and κ-Köhler ($d_{ve,\,fit}$)) and experimental results for $mf_{SOA}(APM) > 0.12$ (Figs. 11 and 12). The κ value varies with the molar mass of SOA. For example, a change of $\pm 0.020\,kg\,mol^{-1}$ in M_{SOA} would change the κ value with ± 0.01. This would result in a change in critical supersaturation of ± 0.01–0.03 (depending on $mf_{SOA}(APM)$, and size of the particle), still close to empirical results.

To summarise, in general the number of ions or water-soluble molecules in the particle determines the point of activation at a certain saturation. However, for the freshly emitted soot agglomerates this approach is only partly true. For these particles, where the un- or semi-soluble material of the dry particle makes up a large part of the volume fraction of the droplet during activation, the material can have a pronounced effect on the activation properties. The organic fraction, the properties of this fraction and to some degree the size of the particle (numbers I, II and III) are represented in theory by κ, i.e. representing the number of ions or water-soluble molecules in the particle. Shape effects, such as size and extent of agglomeration (numbers III and IV), also affect the CCN behaviour of the fresh and slightly processed soot. However, this effect will ebb away as the water-soluble (organic) material coating the particles increases.

5.4 Uncertainties

In the CCNC, the high supersaturations required for measurements of fresh soot or early aged soot are hard to achieve. Furthermore, the first activation scans are difficult to evaluate and do not show full supersaturation spectra. These scans have therefore been excluded here, but they still bring valuable information of the early activation properties. Also, we cannot rule out biases from volatilisation of semi-volatile compounds in the instrument, even though the operation mode of SFCA minimises this effect. As discussed by others (Asa-Awuku et al., 2009; Frosch et al., 2013), part of the material may volatilise inside the column of the instrument due to the large temperatures required for high supersaturation. The effect would be a smaller size of the particle with less hydrophilic content, which would become less CCN active, though the loss of SOA becomes less probable as the droplets form and gets diluted inside the instrument. However, the results from this study sometimes show the opposite effect (e.g. in Fig. 11 there is a discrepancy between empirical results for FSP2 from the two instruments). The two instruments measure at different temperature differences (ΔT) and when higher temperatures are used, the particles are more CCN active. A possible explanation for this could be that the measurements are performed at the end of each calibration curve (i.e. low vs. high flow for different ΔT) and are therefore associated with larger error bars. Another explanation could be that the activation occurs at different positions inside the column; this is something that should be investigated further and hence is not accounted for in this study.

During measurements using the newly developed SFCA the aerosol is subjected to the same temperature difference for each supersaturation scan in each instrument (sometimes overlapping), and thereby also more or less subjected to the same volatilisation loss of the semi-volatile compounds. In the original CFSTGC mode, the temperature difference increase with increased supersaturation, leading to different volatilisation losses during one supersaturation scan (which can be avoided by instead altering the particle diameter). In summary, using the SFCA mode in the CCNC during measurement minimises the volatilisation effect, although we cannot rule out biases totally.

A DMA-TD-APM set-up measures the mass–mobility relationship of the particles. From these measurements the volume-equivalent diameters ($d_{ve,measured}$) as well as the organic and soot mass fractions ($mf_{org}(APM)$ and $mf_{BC}(APM)$, respectively) are derived. Thereafter, the POA and SOA mass fractions ($mf_{POA}(APM)$ and $mf_{SOA}(APM)$, respectively) of the particles are estimated from $mf_{org}(APM)$, as described in the Sect. 4.1. Measurements of the organic fraction (POA) at the beginning of the experiments (before and just after the onset of UV) are stable over size, with an average $mf_{org}(APM) = 3$–$4\,\%$. In general the OA fraction (both POA and SOA) from DMA-TD-APM measurements differs slightly from that measured by SP-AMS, with the assumptions made in this study (for more information regarding the SP-AMS assumptions see the Supplement). Likely the difference is attributed to the OA-properties in relation to the two measurement techniques and the quantification of BC in the SP-AMS. For example, POA may be strongly bound to or within the soot core and may thus be incompletely removed with the thermodenuder. Further, changes in Collection Efficiency (for example laser – particle beam overlap) of the SP-AMS when transforming the soot from aggregated to spherical structure upon aging require further investigation. This should not have a significant effect on the modelling nor when comparing empirical results with modelled ones. In the model, the POA fraction is considered hydrophobic and the

same corrections are made for both the empirical and modelled results (as described below).

Uncertainties from the difficulties of measurements of CCN properties and mass fractions of the particles are inherited in the calculations and models. Firstly, the point of activation of particles inside the CCNC column is unknown. Therefore, the temperature at activation is uncertain. For the largest used ΔT ($= 18$ K) the temperature ranges from 296.15 to 314.15 K in the column. As described before, the absolute temperature ($T = 298.15$ K) and the surface tension of water ($\sigma_{\text{water}} = 0.072$ N m^{-1}) are used for the calibration and the model calculations. These values show good agreement with empirical results and when compared to the temperature range in the column. Secondly, the SOA mass fraction is an approximation, as described earlier. An inaccuracy of mf_{SOA}(APM) will be larger in the early part of the ageing process than in the end, and will have the same effect in the model. Thirdly, for better resolution, mf_{SOA}(APM) data were fitted with sigmoidal functions, which has been used in the model. This approach could cause errors while modelling. On the other hand, the same functions have been used for plotting the cloud-activation data.

6 Conclusions

Diesel exhaust aerosol and soot from a flame soot generator spiked with light aromatic SOA precursors (*m*-xylene and toluene) was photochemically aged. The time-dependent changes of the soot particle were characterised with respect to hygroscopic properties, mass–mobility relationship and chemical composition, with the main focus on CCN properties.

For fresh soot particles no activation into cloud droplets at supersaturations < 2 % is observed. It is unlikely that any substantial SOA formation is taking place before the onset of UV radiation, in dark conditions. At the onset of UV exposure an immediate change in activation properties occurs, with only a small increase of the organic fraction coating the soot particles. At this point more hydrophilic (oxidised) organic compounds, containing e.g. carbonyl, alcohol, carboxylic acid, hydrogen peroxide nitrate and nitro functional groups, are produced. Initially, the SOA formation is probably dominated by low-volatile oxidation products formed from the reactions between OH and IVOCs in the diesel exhausts. However, within an hour after the onset of UV exposure, more volatile oxidation products formed from the added *m*-xylene and toluene also start to condense onto the soot particles. By the end of the experiments (after 4–5 h of photochemical ageing), the SOA is dominated by *m*-xylene and toluene oxidation products. The instantaneous change in CCN properties at the onset of UV-radiation could be attributed to condensation of SOA or it could be an effect of oxidation of the organic material already in the particle phase.

Ageing of soot particles progressively enhances their ability to act as CCN. In summary, the time-dependent changes of activation properties are attributed to the (I) organic fraction of the particle and (II) chemical properties of this fraction, as well as the (III) size and (IV) morphology of the particle. Information of these four parameters (I–IV) is highly relevant when predicting the activation point of the slightly processed soot. However, as the soot ages the shape (IV) effects diminishes.

As expected, there is a size dependency of the activation properties as well as for the mass acquisition of secondary organic material – two effects affecting the activation in this experiment. Smaller particles are harder to activate into cloud droplets, although slightly higher relative mass acquisition of SOA are observed for smaller sizes. The results also indicate that the size of the primary particles and morphology of the fresh soot core might be of importance. Aggregates consisting of primary particles with a smaller diameter (d_{pp}) require a higher supersaturation than aggregates made of larger primary particles at the same SOA mass fraction. On the other hand, aggregates with smaller d_{pp} activate at lower supersaturation compared to particles with larger d_{pp} at certain volume-equivalent diameter (d_{ve}).

POA has been treated as hydrophobic in the CCN modelling, not contributing to any CCN activity. SOA on the other hand enhances the ability of the soot particles to act as a CCN with increasing amount of condensing material. These assumptions seem to be to modest for modelling the cloud droplet formation in the early ageing process. As discussed in Sect. 5.2, the POA may undergo heterogeneous oxidation before the onset of UV exposure, or be oxidised by OH or ozone, which may increase the hygroscopicity of the material – in which case POA (or OPOA) should be treated as slightly hygroscopic. The initial SOA formation might be from condensation of low-volatile organic compounds in the diesel exhaust. The chemical composition would then differ, with slightly different hygroscopic properties than SOA formed from the added precursors as a result. Hence, the early SOA might not be as hygroscopic as the aged one. However, the instantaneous change in CCN properties can most likely be attributed to condensation of SOA. A strong increase of SOA is seen at the beginning of the experiments, accompanied by a similar trend for the increasing volume-equivalent diameter (d_{ve}) and a decrease in critical water vapour supersaturation s_{c}.

The decline in s_{c}, required to activate the organic coated soot particles, can be modelled by κ-Köhler theory accounting for the agglomerated structure of the particles. Information of the volume-equivalent diameter (d_{ve}) or shape factor (χ) is necessary for a good representation. Also needed is the chemical composition (e.g. M, ρ, i) and amount of the organic material (mf or ε). If d_{m} and mf_{SOA} are known, d_{ve} can be calculated from the empirically fitted functions. The model captures the evolution of the activation properties well for mf_{SOA}(APM) > 0.12. Modelling of κ_{sum} (Eq. 7) based

on $\kappa_{SOA} = 0.13$ shows good agreement with κ_{CCN} (Eqs. 9 and 10), with largest deviations for the lowest/highest values ($\kappa < 0.015$ and $\kappa > 0.085$, in Fig. S7b, Supplement). Modelled s_c, when κ_{SOA} is used for the calculations, corresponds well to the s_c measured at the end of the experiments for all sizes ($s_c < 1\,\%$).

The model does not capture the early, steep decrease of the s_c(for $mf_{SOA}(APM) < 0.12$). In reality the slightly coated soot particles are not as good CCN as in the model, which could be explained by a semi-hydrophilic organic layer (with a van't Hoff factor (i) and/or κ_{SOA} value equal or close to zero), hindering effects by shape, and/or unevenly distributed organic material. A limitation in solubility could be an important parameter for CCN activity of atmospheric aerosol particles.

The immediate change in CCN activation at the onset of UV exposure implies that the lifetime of soot in the atmosphere is affected by access to sunlight. Reduced photochemistry, as in wintertime in the Northern Hemisphere, could mean a longer residence time in the atmosphere for soot particles due to prolonged hydrophobicity. That is, soot particles may perturb the radiation budget in the Arctic region due to a longer residence time of the aged particles with enhanced adsorption properties. In the summer, when sunlight is plentiful, the same soot particles may age rapidly and due to enhanced hygroscopicity of the particles the cloud droplet number concentration may increase, changing the cloud cover. Such a change could influence the radiation budget of the region. On the other hand, an increase in hygroscopicity could result in enhanced deposition. During summer photochemical ageing as well as wet removal have been pointed out as having central roles in controlling the properties of the aerosol size distribution. Deposition of soot on the snow surface may in turn change the albedo of the snow surface and thereby influence the climate of the Arctic region.

Change in hygroscopicity and morphology of the ageing soot particles will also affect the deposition of the particles in the human respiratory tract, according to Löndahl et al. (2009).

Appendix A

Table A1. Nomenclature.

Nomenclature	
a_w	Water activity
ADCHAM	Aerosol Dynamics, gas- and particle-phase chemistry model for laboratory CHAMber studies
BC	Black Carbon
C_c	Cunningham correction factor
CCN	Cloud condensation nuclei
CCNC	Cloud condensation nuclei counter
CFSTGC	Continuous-flow streamwise thermal-gradient counter
CPC	Condensational particle counter
DEP	Diesel exhaust particle
d_m	Mobility diameter
$d_{m,dry}$	Mobility diameter of the dry particle
DMA-TD-APM	Differential mobility analyser–aerosol particle mass analyser with a thermodenuder
d_{pp}	Primary particle diameter
d_s	Diameter of the dry particle
DSOA	Dark Secondary organic aerosol
d_{ve}	Volume-equivalent diameter
$d_{ve,fit}$	Calculated volume-equivalent diameter from empirical fit
$d_{ve,measured}$	Volume-equivalent diameter from measurement
d_{wet}	Diameter of the spherical aqueous solution droplet
FSP	Flame soot generator particle
GMD	Geometric mean diameter
HR-ToF-AMS	High-resolution time-of-flight mass spectrometer
i	van't Hoff factor, represents the effects of ion interactions and dissociation
IVOC	Intermediate volatility organic compound
Ke	Kelvin effect
LV-OOA	Low-volatility oxygenated organic aerosol
mf_{org}(APM)	Mass fraction organic from APM measurements (mass–mobility relationship)
mf_{POA}(APM)	Mass fraction POA from APM measurements (mass–mobility relationship)
mf_{SOA}(AMS)	Mass fraction SOA from AMS measurements (chemical composition)
mf_{SOA}(APM)	Mass fraction SOA from APM measurements (mass–mobility relationship)
mf_{BC}(APM)	Mass fraction soot from APM measurements (mass–mobility relationship)
M_i	Molecular mass for a specific component
n_{sum}	Sum of the different contributing components in the particles
O : C ratio	Oxygen to carbon ratio
OA	Organic aerosol
OC	Organic carbon
OPC	Optical particle counter
OPOA	Oxygenated primary organic aerosol
p	Actual partial pressure
P	Pressure
p_o	Equilibrium pressure over a flat surface of pure water
POA	Primary organic aerosol
Q_{50}	Critical flow rate
R	Universal gas constant
s	Saturation ratio
s_c	Critical supersaturation
s_c #52	Critical supersaturation measured by instrument no. 52
SFCA	Scanning flow CCN analysis
SMPS	Scanning mobility particle sizer
SOA	Secondary organic aerosol
SP-AMS	Soot particle aerosol mass spectrometer
SV-OOA	Semi-volatile oxygenated organic aerosol
T	Absolute temperature
TEM	Transmission electron microscope
VOC	Volatile organic compound
Wettable	Model taking only the Kelvin effect into account
ΔT	Streamwise temperature gradient
ε_i	Volume fraction of a specific component in the dry particle
κ	Hygroscopicity parameter describing the number of ions or non-dissociating molecules per unit volume of the dry particle
κ-Köhler	Model using κ-Köhler theory
κ-Köhler(d_m)	Model using κ-Köhler theory, with the d_m as input parameter for d_s
κ-Köhler($d_{ve,fit}$)	Model using κ-Köhler theory, with the fitted d_{ve} as input parameter for d_s
κ-Köhler($d_{ve,measured}$)	Model using κ-Köhler theory, with the empirically derived d_{ve} as input parameter for d_s
κ_{CCN}	Hygroscopicity parameter value derived from the measured critical supersaturation
κ_{SOA}	Hygroscopicity parameter value calculated from chemical composition of SOA
ν	Dissociation number
ρ_{corr}	Corrected material density of the particles
ρ_i	Density of a specific component
ρ_w	Density of water
σ_g	Standard deviation of the geometric mean diameter from the lognormal number size distribution
σ_{sol}	Surface tension of the solution droplet
σ_w	Surface tension of water
ϕ	Molal or practical osmotic coefficient of the solute in aqueous solution
χ	Shape factor

The Supplement related to this article is available online at doi:10.5194/acp-14-9831-2014-supplement.

Acknowledgements. The Swedish Research Council (VR), The Swedish Research Council Formas, ModElling the Regional and Global Earth system – MERGE, ClimBEco research school (Lund University), Aerosols Clouds and Trace gases Research InfraStructure Network – ACTRIS, and Cryosphere-atmosphere interactions in a changing Arctic climate – CRAICC supported this work.

Edited by: H. Skov

References

Ackerman, A. S., Toon, O., Stevens, D., Heymsfield, A., Ramanathan, V., and Welton, E.: Reduction of tropical cloudiness by soot, Science, 288, 1042–1047, 2000.

Albrecht, B. A.: Aerosols, cloud microphysics, and fractional cloudiness, Science, 245, 1227–1230, 1989.

Andreae, M. O. and Rosenfeld, D.: Aerosol-cloud-precipitation interactions. Part 1. The nature and sources of cloud-active aerosols, Earth-Sci. Rev., 89, 13–41, 2008.

Arens, F., Gutzwiller, L., Baltensperger, U., Gaggeler, H. W., and Ammann, M.: Heterogeneous reaction of NO_2 on diesel soot particles, Environ. Sci. Technol. 35, 2191–2199, 2001.

Asa-Awuku, A., Engelhart, G. J., Lee, B. H., Pandis, S. N., and Nenes, A.: Relating CCN activity, volatility, and droplet growth kinetics of β-caryophyllene secondary organic aerosol, Atmos. Chem. Phys., 9, 795–812, doi:10.5194/acp-9-795-2009, 2009.

Bilde, M. and Svenningsson, B.: CCN activation of slightly soluble organics: the importance of small amounts of inorganic salt and particle phase, Tellus B, 56, 128–134, 2004.

Bond, T. C., Doherty, S. J., Fahey, D. W., Forster, P. M., Berntsen, T., DeAngelo, B. J., Flanner, M. G., Ghan, S., Karcher, B., Koch, D., Kinne, S., Kondo, Y., Quinn, P. K., Sarofim, M. C., Schultz, M. G., Schulz, M., Venkataraman, C., Zhang, H., Zhang, S., Bellouin, N., Guttikunda, S. K., Hopke, P. K., Jacobson, M. Z., Kaiser, J. W., Klimont, Z., Lohmann, U., Schwarz, J. P., Shindell, D., Storelvmo, T., Warren, S. G., and Zender, C. S.: Bounding the role of black carbon in the climate system: A scientific assessment, J. Geophys. Res.-Atmos., 118, 5380–5552, 2013.

Canagaratna, M. R., Jayne, J. T., Jimenez, J. L., Allan, J. D., Alfarra, M. R., Zhang, Q., Onasch, T. B., Drewnick, F., Coe, H., Middlebrook, A., Delia, A., Williams, L. R., Trimborn, A. M., Northway, M. J., DeCarlo, P. F., Kolb, C. E., Davidovits, P., and Worsnop, D. R. Chemical and microphysical characterization of ambient aerosols with the aerodyne aerosol mass spectrometer, Mass Spectrom. Rev. 26, 185–222, 2007.

Cappa, C. D., Onasch, T. B., Massoli, P., Worsnop, D. R., Bates, T. S., Cross, E. S., Davidovits, P., Hakala, J., Hayden, K. L., Jobson, B. T., Kolesar, K. R., Lack, D. A., Lerner, B. M., Li, S. M., Mellon, D., Nuaaman, I., Olfert, J. S., Petaja, T., Quinn, P. K., Song, C., Subramanian, R., Williams, E. J., and Zaveri, R. A.: Radiative Absorption Enhancements Due to the Mixing State of Atmospheric Black Carbon, Science, 337, 1078–1081, 2012.

Chan, A. W. H., Kautzman, K. E., Chhabra, P. S., Surratt, J. D., Chan, M. N., Crounse, J. D., Kürten, A., Wennberg, P. O., Flagan, R. C., and Seinfeld, J. H.: Secondary organic aerosol formation from photooxidation of naphthalene and alkylnaphthalenes: implications for oxidation of intermediate volatility organic compounds (IVOCs), Atmos. Chem. Phys., 9, 3049–3060, doi:10.5194/acp-9-3049-2009, 2009.

Chang, R. Y.-W., Slowik, J. G., Shantz, N. C., Vlasenko, A., Liggio, J., Sjostedt, S. J., Leaitch, W. R., and Abbatt, J. P. D.: The hygroscopicity parameter (κ) of ambient organic aerosol at a field site subject to biogenic and anthropogenic influences: relationship to degree of aerosol oxidation, Atmos. Chem. Phys., 10, 5047–5064, doi:10.5194/acp-10-5047-2010, 2010.

Choi, M. Y., A. Hamins, A., Mulholland, G. W., and Kashiwagi, T.: Simultaneous Optical Measurements of Soot Volume Fraction and Temperature in Premixed Flames, Combustion Flame, 99, 174–186, 1994.

Cross, E. S., Slowik, J. G., Davidovits, P., Allan, J. D., Worsnop, D. R., Jayne, J. T., Lewis, D. K., Canagaratna, M., and Onasch, T. B.: Laboratory and ambient particle density determinations using light scattering in conjunction with aerosol mass spectrometry, Aerosol Sci. Tech., 41, 343–359, 2007.

DeCarlo, P. F., Slowik, J. G., Worsnop, D. R., Davidovits, P., and Jimenez, J. L.: Particle morphology and density characterization by combined mobility and aerodynamic diameter measurements. Part 1: Theory, Aerosol Sci. Tech., 38, 1185–1205, 2004.

DeCarlo, P. F., Kimmel, J. R., Trimborn, A., Northway, M. J., Jayne, J. T., Aiken, A. C., Gonin, M., Fuhrer, K., Horvath, T., and Docherty, K. S.: Field-deployable, high-resolution, time-of-flight aerosol mass spectrometer, Anal. Chem., 78, 8281–8289, 2006.

Duplissy, J., Gysel, M., Alfarra, M. R., Dommen, J., Metzger, A., Prevot, A. S. H., Weingartner, E., Laaksonen, A., Raatikainen, T., Good, N., Turner, S. F., McFiggans, G., and Baltensperger, U. "Cloud forming potential of secondary organic aerosol under near atmospheric conditions, Geophys. Res. Lett., 35, L03818, doi:10.1029/2007gl031075, 2008.

Dusek, U., Frank, G. P., Hildebrandt, L., Curtius, J., Schneider, J., Walter, S., Chand, D., Drewnick, F., Hings, S., Jung, D., Borrmann, S., and Andreae, M. O.: Size matters more than chemistry for cloud-nucleating ability of aerosol particles, Science, 312, 1375–1378, 2006.

Donahue, N. M., Robinson, A. L., and Pandis, S. N.: Atmospheric organic particulate matter: From smoke to secondary organic aerosol, Atmos. Environ., 43, 94–106, doi:10.1016/j.atmosenv.2008.09.055, 2009

Florence, A. T., Attwood, D. and Attwood, D. Physicochemical principles of pharmacy Pharmaceutical Press, TJ International, Padstow, Cornwall, UK, 2011.

Frosch, M., Bilde, M., Nenes, A., Praplan, A. P., Jurányi, Z., Dommen, J., Gysel, M., Weingartner, E., and Baltensperger, U.: CCN activity and volatility of β-caryophyllene secondary organic aerosol, Atmos. Chem. Phys., 13, 2283–2297, doi:10.5194/acp-13-2283-2013, 2013.

Gunthe, S. S., King, S. M., Rose, D., Chen, Q., Roldin, P., Farmer, D. K., Jimenez, J. L., Artaxo, P., Andreae, M. O., Martin, S. T., and Pöschl, U.: Cloud condensation nuclei in pristine tropical rainforest air of Amazonia: size-resolved measurements and modeling of atmospheric aerosol composition and CCN activity,

Atmos. Chem. Phys., 9, 7551–7575, doi:10.5194/acp-9-7551-2009, 2009.

Gysel, M., Nyeki, S., Weingartner, E., Baltensperger, U., Giebl, H., Hitzenberger, R., Petzold, A., and Wilson, C. W.: Properties of jet engine combustion particles during the PartEmis experiment: Hygroscopicity at subsaturated conditions, Geophys. Res. Lett., 30, 1566, doi:10.1029/2003gl016896, 2003.

Hallquist, M., Wenger, J. C., Baltensperger, U., Rudich, Y., Simpson, D., Claeys, M., Dommen, J., Donahue, N. M., George, C., Goldstein, A. H., Hamilton, J. F., Herrmann, H., Hoffmann, T., Iinuma, Y., Jang, M., Jenkin, M. E., Jimenez, J. L., Kiendler-Scharr, A., Maenhaut, W., McFiggans, G., Mentel, Th. F., Monod, A., Prévôt, A. S. H., Seinfeld, J. H., Surratt, J. D., Szmigielski, R., and Wildt, J.: The formation, properties and impact of secondary organic aerosol: current and emerging issues, Atmos. Chem. Phys., 9, 5155–5236, doi:10.5194/acp-9-5155-2009, 2009.

Han, C., Liu, Y. C., and He, H.: Role of Organic Carbon in Heterogeneous Reaction of NO_2 with Soot, Environ. Sci. Technol., 47, 3174–3181, 2013.

Hart, J. E., Laden, F., Eisen, E. A., Smith, T. J., and Garshick, E.: Chronic obstructive pulmonary disease mortality in railroad workers, Occup. Environ. Med., 66, 221–226, 2009.

Henning, S., Ziese, M., Kiselev, A., Saathoff, H., Möhler, O., Mentel, T. F., Buchholz, A., Spindler, C., Michaud, V., Monier, M., Sellegri, K., and Stratmann, F.: Hygroscopic growth and droplet activation of soot particles: uncoated, succinic or sulfuric acid coated, Atmos. Chem. Phys., 12, 4525–4537, doi:10.5194/acp-12-4525-2012, 2012.

Hersey, S. P., Craven, J. S., Metcalf, A. R., Lin, J., Lathem, T., Suski, K. J., Cahill, J. F., Duong, H. T., Sorooshian, A., Jonsson, H. H., Shiraiwa, M., Zuend, A., Nenes, A., Prather, K. A., Flagan, R. C., and Seinfeld, J. H.: Composition and hygroscopicity of the Los Angeles Aerosol: CalNex, J. Geophys. Res.-Atmos., 118, 3016–3036, 2013.

Huff Hartz, K. E., Rosenørn, T., Ferchak, S. R., Raymond, T. M., Bilde, M., Donahue, N. M., and Pandis, S. N.: Cloud condensation nuclei activation of monoterpene and sesquiterpene secondary organic aerosol, J. Geophys. Res.-Atmos., 110, D14208, doi:10.1029/2004JD005754, 2005.

IPCC: Climate Change 2007: The Physical Science Basis. Contribution of Working Group I to the Fourth Assessment Report of the Intergovernmental Panel on Climate Change, 2007.

IPCC: Climate Change 2013: The Physical Science Basis. Working Group I Contribution to the IPCC 5th Assessment Report – Changes to the Underlying Scientific/Technical Assessment (IPCC-XXVI/Doc.4), 2013.

Jenkin, M. E., Saunders, S. M., Wagner, V., and Pilling, M. J.: Protocol for the development of the Master Chemical Mechanism, MCM v3 (Part B): tropospheric degradation of aromatic volatile organic compounds, Atmos. Chem. Phys., 3, 181–193, doi:10.5194/acp-3-181-2003, 2003.

Jimenez, J. L., Canagaratna, M. R., Donahue, N. M., Prevot, A. S. H., Zhang, Q., Kroll, J. H., DeCarlo, P. F., Allan, J. D., Coe, H., Ng, N. L., Aiken, A. C., Docherty, K. S., Ulbrich, I. M., Grieshop, A. P., Robinson, A. L., Duplissy, J., Smith, J. D., Wilson, K. R., Lanz, V. A., Hueglin, C., Sun, Y. L., Tian, J., Laaksonen, A., Raatikainen, T., Rautiainen, J., Vaattovaara, P., Ehn, M., Kulmala, M., Tomlinson, J. M., Collins, D. R., Cubison, M. J., Dunlea, E. J., Huffman, J. A., Onasch, T. B., Alfarra, M. R., Williams, P. I., Bower, K., Kondo, Y., Schneider, J., Drewnick, F., Borrmann, S., Weimer, S., Demerjian, K., Salcedo, D., Cottrell, L., Griffin, R., Takami, A., Miyoshi, T., Hatakeyama, S., Shimono, A., Sun, J. Y., Zhang, Y. M., Dzepina, K., Kimmel, J. R., Sueper, D., Jayne, J. T., Herndon, S. C., Trimborn, A. M., Williams, L. R., Wood, E. C., Middlebrook, A. M., Kolb, C. E., Baltensperger, U., and Worsnop, D. R.: Evolution of Organic Aerosols in the Atmosphere, Science, 326, 1525–1529, 2009.

Kanakidou, M., Seinfeld, J. H., Pandis, S. N., Barnes, I., Dentener, F. J., Facchini, M. C., Van Dingenen, R., Ervens, B., Nenes, A., Nielsen, C. J., Swietlicki, E., Putaud, J. P., Balkanski, Y., Fuzzi, S., Horth, J., Moortgat, G. K., Winterhalter, R., Myhre, C. E. L., Tsigaridis, K., Vignati, E., Stephanou, E. G., and Wilson, J.: Organic aerosol and global climate modelling: a review, Atmos. Chem. Phys., 5, 1053–1123, doi:10.5194/acp-5-1053-2005, 2005.

Khalizov, A. F., Zhang, R. Y., Zhang, D., Xue, H. X., Pagels, J., and McMurry, P. H.: Formation of highly hygroscopic soot aerosols upon internal mixing with sulfuric acid vapor, J. Geophys. Res.-Atmos., 114, doi:10.1029/2008JD010595, 2009.

Kreidenweis, S. M., Koehler, K., DeMott, P. J., Prenni, A. J., Carrico, C., and Ervens, B.: Water activity and activation diameters from hygroscopicity data – Part I: Theory and application to inorganic salts, Atmos. Chem. Phys., 5, 1357–1370, doi:10.5194/acp-5-1357-2005, 2005.

Kroll, J. H., Donahue, N. M., Jimenez, J. L., Kessler, S. H., Canagaratna, M. R., Wilson, K. R., Altieri, K. E., Mazzoleni, L. R., Wozniak, A. S., Bluhm, H., Mysak, E. R., Smith, J. D., Kolb, C. E., and Worsnop, D. R.: Carbon oxidation state as a metric for describing the chemistry of atmospheric organic aerosol, Nat. Chem., 3, 133–139, 2011.

Kundu, S., Fisseha, R., Putman, A. L., Rahn, T. A., and Mazzoleni, L. R.: High molecular weight SOA formation during limonene ozonolysis: insights from ultrahigh-resolution FT-ICR mass spectrometry characterization, Atmos. Chem. Phys., 12, 5523–5536, doi:10.5194/acp-12-5523-2012, 2012.

Kuwata, M., Shao, W., Lebouteiller, R., and Martin, S. T.: Classifying organic materials by oxygen-to-carbon elemental ratio to predict the activation regime of Cloud Condensation Nuclei (CCN), Atmos. Chem. Phys., 13, 5309–5324, doi:10.5194/acp-13-5309-2013, 2013.

Köhler, H.: The Nucleus in and the Growth of Hygroscopic Droplets, T. Faraday Soc., 32, 1152–1161, 1936.

Laaksonen, A., Korhonen, P., Kulmala, M., and Charlson, R. J.: Modification of the Kuhler equation to include soluble trace gases and slightly soluble substances, J. Atmos. Sci., 55, 853–862, 1998.

Lambe, A. T., Onasch, T. B., Massoli, P., Croasdale, D. R., Wright, J. P., Ahern, A. T., Williams, L. R., Worsnop, D. R., Brune, W. H., and Davidovits, P.: Laboratory studies of the chemical composition and cloud condensation nuclei (CCN) activity of secondary organic aerosol (SOA) and oxidized primary organic aerosol (OPOA), Atmos. Chem. Phys., 11, 8913–8928, doi:10.5194/acp-11-8913-2011, 2011.

Lance, S., Medina, J., Smith, J. N., and Nenes, A.: Mapping the operation of the DMT Continuous Flow CCN counter, Aerosol Sci. Tech., 40, 242–254, 2006.

Lide, D. R.: Physical Constants of Organic Compounds, in: CRC Handbook of Chemistry and Physics, Internet Version 2005, CRC Press, Boca Raton, FL, available at: http://www.hbcpnetbase.com (last access: 10 December 2013), 2005.

Löndahl, J., Pagels, J., Boman, C., Swietlicki, E., Massling, A., Rissler, J., Blomberg, A., Bohgard, M., and Sandström, T.: Deposition of biomass combustion aerosol particles in the human respiratory tract, Inhal. Toxicol., 20, 923–933, 2008.

Löndahl, J., Massling, A., Swietlicki, E., Bräuner, E. V., Ketzel, M., Pagels, J., and Loft, S.: Experimentally determined human respiratory tract deposition of airborne particles at a busy street, Environ. Sci. Technol., 43, 4659–4664, 2009.

Malik, A., Abdulhamid, H., Pagels, J., Rissler, J., Lindskog, M., Nilsson, P., Bjorklund, R., Jozsa, P., Visser, J., Spetz, A., and Sanati, M.: A Potential Soot Mass Determination Method from Resistivity Measurement of Thermophoretically Deposited Soot, Aerosol Sci. Tech., 45, 284–294, 2011.

Maricq, M. M. and Ning, X. "The effective density and fractal dimension of soot particles from premixed flames and motor vehicle exhaust, J. Aerosol Sci., 35, 1251–1274, 2004.

McMurry, P. H., Wang, X., Park, K., and Ehara, K.: The relationship between mass and mobility for atmospheric particles: A new technique for measuring particle density, Aerosol Sci. Tech., 36, 227–238, 2002.

Meyer, N. K. and Ristovski, Z. D.: Ternary nucleation as a mechanism for the production of diesel nanoparticles: Experimental analysis of the volatile and hygroscopic properties of diesel exhaust using the volatilization and humidification tandem differential mobility analyzer, Environ. Sci. Technol., 41, 7309–7314, 2007.

Mills, N. L., Törnqvist, H., Gonzalez, M. C., Vink, E., Robinson, S. D., Söderberg, S., Boon, N. A., Donaldson, K., Sandström, T., and Blomberg, A.: Ischemic and thrombotic effects of dilute diesel-exhaust inhalation in men with coronary heart disease, New Engl. J. Med., 357, 1075–1082, 2007.

Moore, R. H. and Nenes, A.: Scanning Flow CCN Analysis – A Method for Fast Measurements of CCN Spectra, Aerosol Sci. Tech., 43, 1192–1207, 2009.

Nakao, S., Shrivastava, M., Nguyen, A., Jung, H., and Cocker, D.: Interpretation of Secondary Organic Aerosol Formation from Diesel Exhaust Photooxidation in an Environmental Chamber, Aerosol Sci. Tech., 45, 964–972, 2011.

Ng, N. L., Kroll, J. H., Chan, A. W. H., Chhabra, P. S., Flagan, R. C., and Seinfeld, J. H.: Secondary organic aerosol formation from *m*-xylene, toluene, and benzene, Atmos. Chem. Phys., 7, 3909–3922, doi:10.5194/acp-7-3909-2007, 2007.

Nordin, E. Z., Eriksson, A. C., Roldin, P., Nilsson, P. T., Carlsson, J. E., Kajos, M. K., Hellén, H., Wittbom, C., Rissler, J., Löndahl, J., Swietlicki, E., Svenningsson, B., Bohgard, M., Kulmala, M., Hallquist, M., and Pagels, J. H.: Secondary organic aerosol formation from idling gasoline passenger vehicle emissions investigated in a smog chamber, Atmos. Chem. Phys., 13, 6101–6116, doi:10.5194/acp-13-6101-2013, 2013.

Onasch, T., Trimborn, A., Fortner, E., Jayne, J., Kok, G., Williams, L., Davidovits, P., and Worsnop, D.: Soot particle aerosol mass spectrometer: development, validation, and initial application, Aerosol Sci. Tech., 46, 804–817, 2012.

Pagels, J., Khalizov, A. F., McMurry, P. H., and Zhang, R. Y.: Processing of Soot by Controlled Sulphuric Acid and Water CondensationMass and Mobility Relationship, Aerosol Sci. Tech., 43, 629–640, 2009.

Park, K., Cao, F., Kittelson, D. B., and McMurry, P. H.: "Relationship between particle mass and mobility for diesel exhaust particles, Environ. Sci. Technol., 37, 577–583, 2003.

Petters, M. D. and Kreidenweis, S. M.: A single parameter representation of hygroscopic growth and cloud condensation nucleus activity, Atmos. Chem. Phys., 7, 1961–1971, doi:10.5194/acp-7-1961-2007, 2007.

Petters, M. D. and Kreidenweis, S. M.: A single parameter representation of hygroscopic growth and cloud condensation nucleus activity – Part 2: Including solubility, Atmos. Chem. Phys., 8, 6273–6279, doi:10.5194/acp-8-6273-2008, 2008.

Petzold, A., Ogren, J. A., Fiebig, M., Laj, P., Li, S.-M., Baltensperger, U., Holzer-Popp, T., Kinne, S., Pappalardo, G., Sugimoto, N., Wehrli, C., Wiedensohler, A., and Zhang, X.-Y.: Recommendations for reporting "black carbon" measurements, Atmos. Chem. Phys., 13, 8365–8379, doi:10.5194/acp-13-8365-2013, 2013.

Pincus, R. and Baker, M. B.: Effect of precipitation on the albedo susceptibility of clouds in the marine boundary layer, Nature, 372, 250–252, 1994.

Pöschl, U., Rose, D., and Andreae, M. O.: Part 2: Particle Hygroscopicity and Cloud Condensation Nucleus Activity, Clouds in the Perturbed Climate System: Their Relationship to Energy Balance, Atmospheric Dynamics, and Precipitation 58–72, 2009.

Prenni, A. J., Petters, M. D., Kreidenweis, S. M., DeMott, P. J., and Ziemann, P. J.: Cloud droplet activation of secondary organic aerosol, J. Geophys. Res.-Atmos., 112, D10223, doi:10.1029/2006jd007963, 2007.

Pruppacher, H. R. and Klett, J. D.: Microphysics of Clouds and Precipitation, Atmospheric and oceanographic sciences library, Kluwer Academic Puplishers, Dordrecht, the Netherlands, 2nd Edn., ISBN:0-7923-4211-9, 1997

Rissler, J., Swietlicki, E., Zhou, J., Roberts, G., Andreae, M. O., Gatti, L. V., and Artaxo, P.: Physical properties of the submicrometer aerosol over the Amazon rain forest during the wet-to-dry season transition – comparison of modeled and measured CCN concentrations, Atmos. Chem. Phys., 4, 2119–2143, doi:10.5194/acp-4-2119-2004, 2004.

Rissler, J., Vestin, A., Swietlicki, E., Fisch, G., Zhou, J., Artaxo, P., and Andreae, M. O.: Size distribution and hygroscopic properties of aerosol particles from dry-season biomass burning in Amazonia, Atmos. Chem. Phys., 6, 471–491, doi:10.5194/acp-6-471-2006, 2006.

Rissler, J., Svenningsson, B., Fors, E. O., Bilde, M., and Swietlicki, E.: An evaluation and comparison of cloud condensation nucleus activity models: predicting particle critical saturationfrom growth at subsaturation, J. Geophys. Res., 115, D22208, doi:10.1029/2010jd014391, 2010.

Rissler, J., Swietlicki, E., Bengtsson, A., Boman, C., Pagels, J., Sandström, T., Blomberg, A., and Löndahl, J.: Experimental determination of deposition of diesel exhaust particles in the human respiratory tract, J. Aerosol Sci., 48, 18–33, 2012.

Rissler, J., Messing, M. E., Malik, A. I., Nilsson, P. T., Nordin, E. Z., Bohgard, M., Sanati, M., and Pagels, J. H.: Effective Density Characterization of Soot Agglomerates from Various Sources and Comparison to Aggregation Theory, Aerosol Sci. Tech., 47, 792–805, 2013.

Rissler, J., Nordin, E. Z., Eriksson, A. C., Nilsson, P. T., Frosch, M., Sporre, M. K., Wierzbicka, A., Svenningsson, B., Löndahl, J., Messing, M. E., Sjogren, S., Hemmingsen, J. G., Loft, S., Pagels, J. H., and Swietlicki, E.: Effective density and mixing state of aerosol particles in a near-traffic urban environment, Environ. Sci. Technol., 48, 6300–6308, doi:10.1021/es5000353, 2014.

Ristimaki, J., Vaaraslahti, K., Lappi, M., and Keskinen, J.: Hydrocarbon condensation in heavy-duty diesel exhaust, Environ. Sci. Technol., 41, 6397–6402, 2007.

Roberts, G. C. and Nenes, A.: A Continuous-Flow Streamwise Thermal-Gradient CCN Chamber for Atmospheric Measurements, Aerosol Sci. Tech., 39, 206–221, 2005.

Roldin, P., Eriksson, A. C., Nordin, E. Z., Hermansson, E., Mogensen, D., Rusanen, A., Boy, M., Swietlicki, E., Svenningsson, B., Zelenyuk, A., and Pagels, J.: Modelling non-equilibrium secondary organic aerosol formation and evaporation with the aerosol dynamics, gas- and particle-phase chemistry kinetic multilayer model ADCHAM, Atmos. Chem. Phys., 14, 7953–7993, doi:10.5194/acp-14-7953-2014, 2014.

Rose, D., Wehner, B., Ketzel, M., Engler, C., Voigtländer, J., Tuch, T., and Wiedensohler, A.: Atmospheric number size distributions of soot particles and estimation of emission factors, Atmos. Chem. Phys., 6, 1021–1031, doi:10.5194/acp-6-1021-2006, 2006.

Rose, D., Gunthe, S. S., Mikhailov, E., Frank, G. P., Dusek, U., Andreae, M. O., and Pöschl, U.: Calibration and measurement uncertainties of a continuous-flow cloud condensation nuclei counter (DMT-CCNC): CCN activation of ammonium sulfate and sodium chloride aerosol particles in theory and experiment, Atmos. Chem. Phys., 8, 1153–1179, doi:10.5194/acp-8-1153-2008, 2008.

Rose, D., Nowak, A., Achtert, P., Wiedensohler, A., Hu, M., Shao, M., Zhang, Y., Andreae, M. O., and Pöschl, U.: Cloud condensation nuclei in polluted air and biomass burning smoke near the mega-city Guangzhou, China – Part 1: Size-resolved measurements and implications for the modeling of aerosol particle hygroscopicity and CCN activity, Atmos. Chem. Phys., 10, 3365–3383, doi:10.5194/acp-10-3365-2010, 2010.

Schauer, J. J., Kleeman, M. J., Cass, G. R., and Simoneit, B. R. T.: Measurement of emissions from air pollution sources. 2. C-1 through C-30 organic compounds from medium duty diesel trucks, Environ. Sci. Technol., 33, 1578–1587, 1999.

Seinfeld, J. H. and Pandis, S. N.: Atmospheric chemistry and physics. From air pollution to climate change, 2nd Edn., John Wiley & Sons, Inc., Hoboken, New Jersey, 2006.

Shinozuka, Y., Clarke, A. D., DeCarlo, P. F., Jimenez, J. L., Dunlea, E. J., Roberts, G. C., Tomlinson, J. M., Collins, D. R., Howell, S. G., Kapustin, V. N., McNaughton, C. S., and Zhou, J.: Aerosol optical properties relevant to regional remote sensing of CCN activity and links to their organic mass fraction: airborne observations over Central Mexico and the US West Coast during MILAGRO/INTEX-B, Atmos. Chem. Phys., 9, 6727–6742, doi:10.5194/acp-9-6727-2009, 2009.

Stubington, J. F., Sergeant, G. D., Barrett, D., Do, P. T. D. H., and Raval, K. A.: Molecular-Weight Determination in the Study of the Lubricating Oil Potential of Shale Oils, Fuel, 74, 79–82, 1995.

Svenningsson, B., Rissler, J., Swietlicki, E., Mircea, M., Bilde, M., Facchini, M. C., Decesari, S., Fuzzi, S., Zhou, J., Mønster, J., and Rosenørn, T.: Hygroscopic growth and critical supersaturations for mixed aerosol particles of inorganic and organic compounds of atmospheric relevance, Atmos. Chem. Phys., 6, 1937–1952, doi:10.5194/acp-6-1937-2006, 2006.

Sydbom, A., Blomberg, A., Parnia, S., Stenfors, N., Sandström, T., and Dahlen, S.: Health effects of diesel exhaust emissions, European Respiratory Journal, 17, 733–746, 2001.

Tree, D. R. and Svensson, K. I.: Soot processes in compression ignition engines, Prog. Energ. Combust., 33, 272–309, 2007.

Tritscher, T., Jurányi, Z., Martin, M., Chirico, R., Gysel, M., Heringa, M. F., DeCarlo, P. F., Sierau, B., Prévôt, A. S. H., Weingartner, E., and Baltensperger, U.: Changes of hygroscopicity and morphology during ageing of diesel soot, Environ. Res. Lett., 6, 034026, doi:10.1088/1748-9326/6/3/034026, 2011.

Tunved, P., Ström, J., and Krejci, R.: Arctic aerosol life cycle: linking aerosol size distributions observed between 2000 and 2010 with air mass transport and precipitation at Zeppelin station, Ny-Ålesund, Svalbard, Atmos. Chem. Phys., 13, 3643–3660, doi:10.5194/acp-13-3643-2013, 2013.

Twomey, S.: Pollution and the planetary albedo: Atmos. Environ., 8, 1251–1256, 1974.

Weingartner, E., Burtscher, H., and Baltensperger, U.: Hygroscopic properties of carbon and diesel soot particles, Atmos. Environ., 31, 2311–2327, 1997.

WHO: Public Health Round-Up: Diesel Exhaust Carcinogenic, Bulletin of the World Health Organization, 477–556, available at: http://www.ncbi.nlm.nih.govpmc/articles/PMC3397708/ (last access: 16 August 2012), 2012.

Wu, Z. J., Poulain, L., Henning, S., Dieckmann, K., Birmili, W., Merkel, M., van Pinxteren, D., Spindler, G., Müller, K., Stratmann, F., Herrmann, H., and Wiedensohler, A.: Relating particle hygroscopicity and CCN activity to chemical composition during the HCCT-2010 field campaign, Atmos. Chem. Phys., 13, 7983–7996, doi:10.5194/acp-13-7983-2013, 2013.

Zhang, R., Khalizov, A. F., Pagels, J., Zhang, D., Xue, H., and McMurry, P. H.: Variability in morphology, hygroscopicity, and optical properties of soot aerosols during atmospheric processing, P. Natl. Acad. Sci. USA, 105, 10291–10296, 2008.